Validation of a Digital Twin for a Ship Engine Cooling System

Joachim Hammarström

Master's thesis in Process and Systems Engineering
Supervisors: Jari Böling, Mikael Manngård and Jerker Björkqvist
Process Control Laboratory
Faculty of Science and Engineering
Åbo Akademi University
Turku, Finland, 2020

Acknowledgements

I would like to thank Jerker Björkqvist at Åbo Akademi University and Farbod Raubetean at Meyer Turku for the opportunity to write this thesis.

I would like to thank Mikael Manngård at Åbo Akademi University for helping me model the engine cooling system and coming with ideas for the thesis. I am also grateful for all his feedback during the thesis process.

I would also like to thank Jari Böling at Åbo Akademi University for helping me with the engine cooling system and Wilhelm Gustafsson at Meyer Turku for helping me when I had questions about the ship data.

I would also like to thank my family for supporting me.

Turku, April 2020

Joachim Hammarström

Abstract

The energy efficiency of ships is becoming more and more important due to increasingly stringent international maritime regulations and rising fuel cost. While many methods have already been put in use that increases the efficiency of some parts of the ship's energy system, the whole power plant has not received much attention.

In this thesis, data taken from a ship was used to modify and adapt a model of a ship engine cooling system made in Simulink which was then validated.

The results show that even with relatively limited data and a quite simple model, it is possible to simulate the cooling system of a ship's engine quite well. Of the three available temperature measurements, the model was reliably able to simulate two of them while the third had a few issues.

Key words: engine cooling system, dynamic simulation, cruise ship, Simulink, Matlab

Abbreviations

DG1	Diesel Generator 1 or Main Engine 1
DG3	Diesel Generator 3 or Main Engine 3
GT	Gross tonnage, a nonlinear way to measure the internal volume of a ship
HFSO	High sulphur fuel oil, maximum 3.50 mass-% sulphur
LNG	Liquefied natural gas
MGO	Marine gas oil
SO_x	Sulphur oxides
ULSFO	Ultra low sulphur fuel oil, maximum 0.10 mass-% sulphur
VLSFO	Very low sulphur fuel oil, maximum 0.50 mass-% sulphur

Contents

1 Introduction

Energy efficiency is becoming more and more important for ship owners, builders, and researchers due to both increasingly strict international maritime regulations and rising fuel cost. All ships over 400 GT built after 1 January 2013 have to follow the new Energy Efficiency Design Index (EEDI) enforced by the International Maritime Organization (IMO) to lower CO_2 emissions by reducing fuel consumption. The EEDI will become stricter every five years beginning in 2015, which means continuous development is required to keep up with the regulations. This makes new ships more expensive to build, but it is expected that the fuel savings will make up for the extra investment cost (IMO, n.da.; ICCT, 2011).

On 1 January 2020, the emission limit for SO_x and particulate matter was drastically reduced outside of Sulphur Emission Control Areas (SECA), from 3.50 mass-% to 0.50 mass-%. Inside of SECAs, the limit has been 0.10 mass-% since 1 January 2015 (IMO, n.db.). This forces ship operators to either install exhaust gas scrubbers or buy fuel with lower sulphur content. Ships with exhaust gas scrubbers installed can continue to use cheap fuel with high sulphur content (HFSO). Other ships will have to use more expensive fuel oils such as VLSFO or ULSFO, or distillates such as MGO, which is even more expensive, to meet the new regulations. Ships with gas engines or dual-fuel engines in gas mode already conform to regulations since LNG does not contain sulphur. The fuel price increase caused by this regulation is another reason why the maritime industry is focusing more and more on energy efficiency.

According to (Zou, et al., 2013), there are many different methods by which fuel efficiency can be improved. Some examples are weather routing, speed optimisation and efficient operation. The most important role in the fuel energy utilisation is of course played by the marine engine itself, since it is the heart of the power plant of the ship. Many methods have already been put into use to improve the energy efficiency of the engine, for example, direct fuel injection, turbocharging, waste heat recovery, etc. These methods, however, are primarily focused on some specific parts while the whole power plant of the ship has not received much attention.

The goal of this thesis is to try and remedy that by adapting and then validating a simple digital twin of a cruise ship's engine cooling system to data obtained from that particular ship. Another goal is to provide insight into what data is needed to run a dynamic simulation of the model, since the provided model only uses static inputs. As heat exchangers are a key component of the cooling system, the primary focus is put on simulating them.

This digital twin can then be used to see how the cooling system reacts to changes in setpoints, parameters, flows, etc. In the future, digital twins will be used on ships in real time to try and optimise the operation of the entire power plant (Manngård, et al., 2020).

1.1 The ship

The ship from which the data was taken is a modern, medium-sized cruise ship. It has two pairs of large, medium-speed diesel engines with different cylinder counts. The ship is referred to as the "reference ship" in the thesis.

1.2 Delimitation

Due to the engine cooling system being very dependent on preheating using the waste heat recovery system when the engine is not running, it was decided to focus on simulating the cooling system during operation. Thus, the results during the time periods when the engine is not running are mostly ignored in this thesis.

2 Literature review

2.1 Digital twins

A digital twin is a virtual copy of a physical process, system, or product. It is constructed to act as a bridge between the physical and the digital world. Using real-world measurements gathered by sensors from a physical system, a digital copy of the system can be built. This model can then be used to, for example, analyse or optimise the real system (Monteith, 2019; Shaw & Fruhlinger, 2019).

2.2 History of the digital twin

While the common belief is that the phrase “digital twin” was first mentioned by the actor Alan Alda in 1998 when referring to a digital copy of his voice in Alan Alda meets Alan Alda 2.0 (Miskinis, 2019), it had actually been used several times before. For example, in (Glos, 1997) it refers to a digital copy of a book that highlighted traces, such as notes and coffee stains, that could then through manipulation be seen on another physical version of the same book. In (Hernández & Hernández, 1997) it refers to a model of a building project where changes were made on the project based on the results of the building of its digital model. The changes were applied to the digital version, then checked, then applied to the construction and so on. This is quite close to the modern usage of the term “digital twin”.

The concept of having a copy of an object or system, albeit physical due to the technology at the time, has been practised since the 1960s. A physical copy of Apollo 13 played a key role in the rescue mission of the real Apollo 13 in April 1970, since it allowed engineers on the ground to test possible solutions to the issues the crew faced (Miskinis, 2019).

The modern concept of a digital equivalent of a physical product was introduced by Dr. Michael Grieves in 2002 during a course on Product Lifecycle Management (PLM) (Grieves & Vickers, 2017). Figure 1 shows the slide used in the presentation.

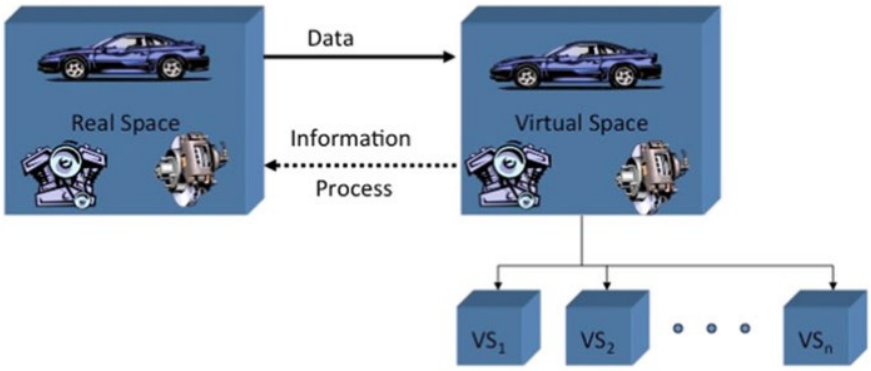

Figure 1 Conceptual ideal for PLM (Grieves & Vickers, 2017)

While it was not called a digital twin at the time, it had all the elements of one: physical model, virtual model and a link for data to flow between the models. In the mid-2000s, it was referred to as the Mirrored Spaces Model and Information Mirroring Model according to (Grieves & Vickers, 2017). In (Grieves, 2011) the concept, while still called Information Mirroring Model, was expanded and the term, Digital Twin, was attached to it. This was done in reference to the way John Vickers, who was Grieves co-author, described the model, although NASA had already called it Digital Twin in 2010 (Shafto, et al., 2010; Piascik, et al., 2010).

During the next few years, there was not much interest in digital twins. (Google Trends, 2019) and (Google Scholar, 2019) show that there were only a few searches and mentions until 2016. However, it was not until 2017 that the interest really started to show. Figure 2 shows the large increase in number of articles that feature “digital twin” in the title in the last few years. While not shown, the relative number of searches according to Google Trends is very similar.

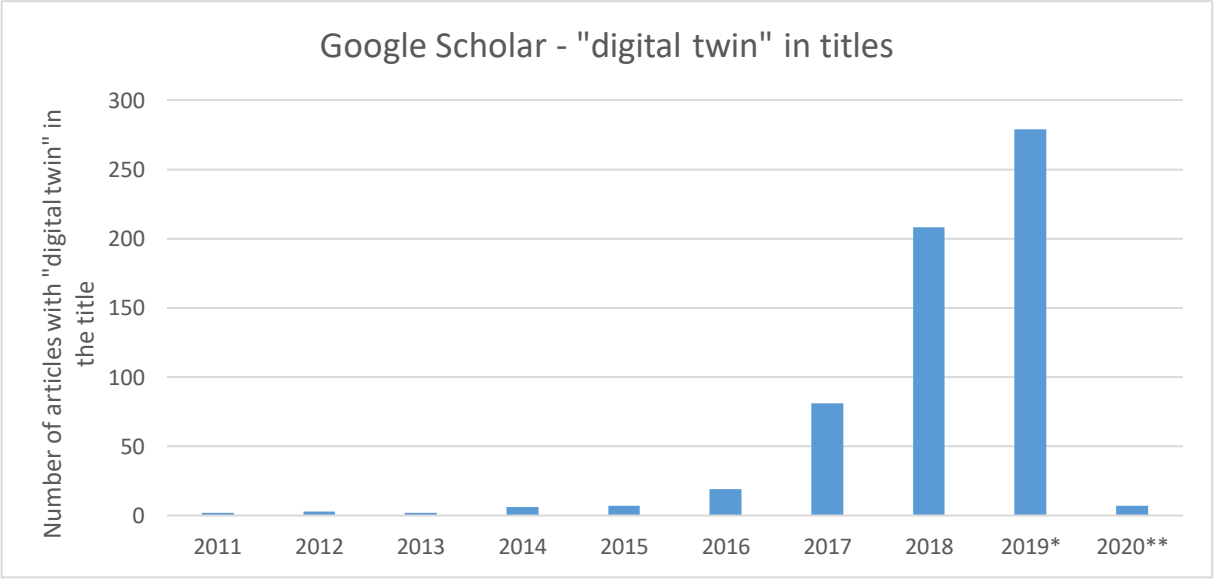

Figure 2 Number of articles on Google Scholar with "digital twin" in the title (Google Scholar, 2019)
**Until 27 September 2019 **Online pre-publication or journal with 2020 copyright*

3 Heat exchanger theory

A ship engine cooling system can, for the most part, be considered a network of interconnected heat exchangers. Hence, in this section, a brief review of the most common types of heat exchangers used in industry is presented. To ensure that the heat exchanger models implemented in the digital twin are able to capture both the steady-state and dynamical behaviour of the physical system, whilst having a complexity suitable for realtime computations, a method of determining the appropriate model complexity is proposed in Section 3.3.4.

A heat exchanger is a device that transfers heat between two or more fluids (liquid or gas) at different temperatures. Due to the second law of thermodynamics, thermal energy always flows from the hot fluid to the cold fluid unless external work is applied. In most heat exchangers, the fluids are separated by some kind of wall. However, there are also heat exchangers where the fluids are in direct contact with each other. Some typical applications for heat exchangers in the marine and energy industry are heating or cooling a certain flow to a specific temperature, rejecting or recovering heat, or evaporation or condensation of single- or multicomponent flows.

There are many different types of heat exchangers and these can be classified in different ways. According to (Shah & Sekulić, 2003), heat exchangers can be classified according to construction features, flow arrangements, transfer processes, number of fluids, degree of surface compactness, and heat transfer mechanisms. The main methods of classification are construction features and flow arrangements.

3.1 Types of heat exchanger construction

Even though there are many different types of heat exchangers, most of them fall into one of two categories: shell and tube, or plate (U.S. Department of Energy, 1993). There is also a third type that is relatively common among small companies due to it being simple and cheap, the double-pipe heat exchanger (Nuclear Power, n.d.; STI, 2014).

3.1.1 Shell and tube

The shell and tube heat exchanger (Figure 3) is the most common heat exchanger in industrial applications. It consists of a shell that contains a large number of tubes that are parallel to the shell. One fluid flows through the tubes while the other flows between the tubes inside the shell allowing heat transfer to take place. Baffles are usually installed in the shell to enhance heat transfer, since they force the shell-side fluid to flow across the shell. A disadvantage of the shell and tube heat exchanger

is that it is relatively large and heavy, which means it is not suitable for automotive and aircraft applications (Çengel & Ghajar, 2015).

Shell and tube heat exchangers can be further classified according to how many shell and tube passes there are in the heat exchanger. Heat exchangers where the tubes make a U-turn in the shell are called one-shell pass and two-tube pass heat exchangers. Similarly, if it has two shell passes and four tube passes it is called a two-shell pass and four-tube pass heat exchanger (Çengel & Ghajar, 2015).

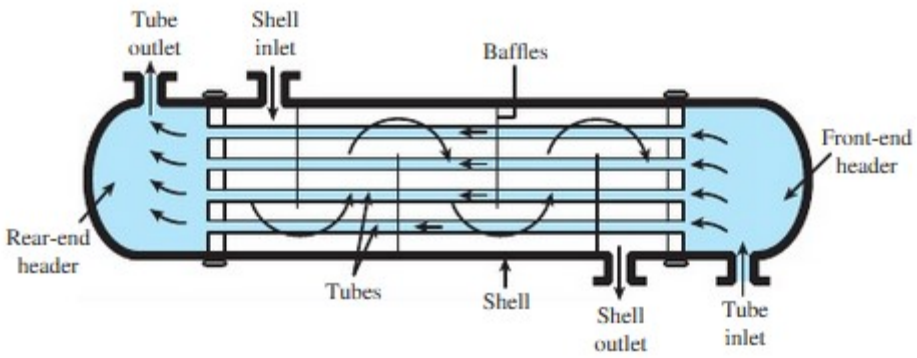

Figure 3 Shell and tube heat exchanger schematic (one-shell and one-tube pass) (Çengel & Ghajar, 2015)

3.1.2 Plate

Another common type of heat exchanger is the plate (or plate and frame) heat exchanger (Figure 4). It has plates instead of tubes to separate the fluids. The fluids alternate between each of the plates so that every other gap has cold fluid flowing through while the rest have a flow of hot fluid. This means that every stream of cold fluid is surrounded by two streams of hot fluid, which results in effective heat transfer. The flow between plates is directed by baffles. Plate heat exchangers are usually smaller than shell and tube heat exchangers of the same capacity due to the high heat transfer efficiency of the plates (Çengel & Ghajar, 2015).

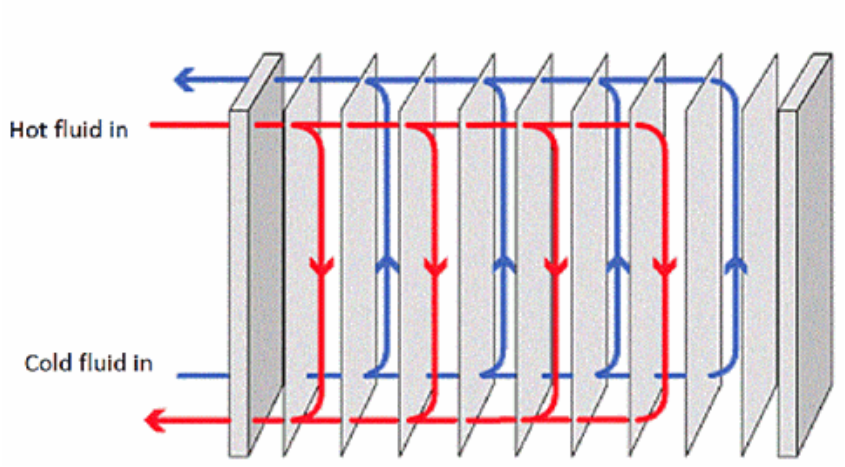

Figure 4 Plate and frame heat exchanger schematic (IPIECA, 2014)

3.1.3 Double-pipe heat exchanger

The simplest and most basic type of heat exchanger is the double-pipe heat exchanger (Figure 5). It consists of two concentric pipes that have different diameters. One fluid flows inside the inner pipe, while the other flows through the annular space between both pipes (Çengel & Ghajar, 2015). They are cheap to build, design and maintain which make them popular in small companies. They are, however, not very efficient and require a large amount of space (STI, 2014).

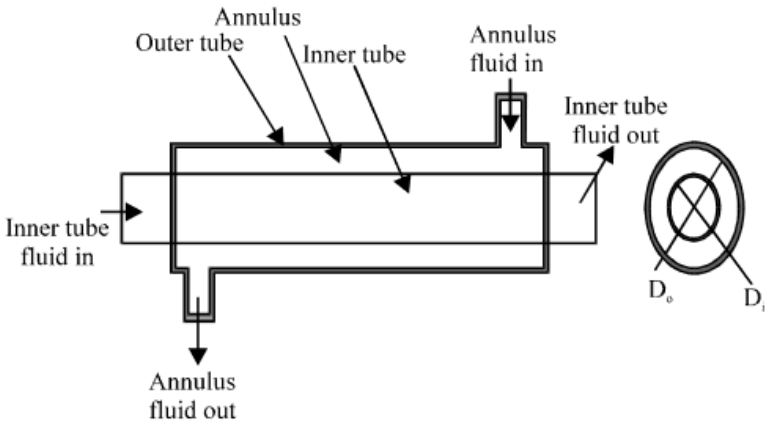

Figure 5 Double pipe heat exchanger (Ramahlingam & Raghavan, 2011)

3.2 Types of heat exchanger flow arrangements

A common characteristic used to categorize heat exchangers is the direction of the two fluid flows relative to each other. The four basic flow arrangements are counter-flow, parallel-flow, cross-flow and hybrids such as cross/counter flow.

3.2.1 Parallel-flow

In parallel-flow (Figure 6) heat exchangers, both the shell fluid and the tube fluid flow parallel to each other in the same direction. The output temperature of the cold flow will approach the output temperature of the hot flow, but will never go higher (U.S. Department of Energy, 1993).

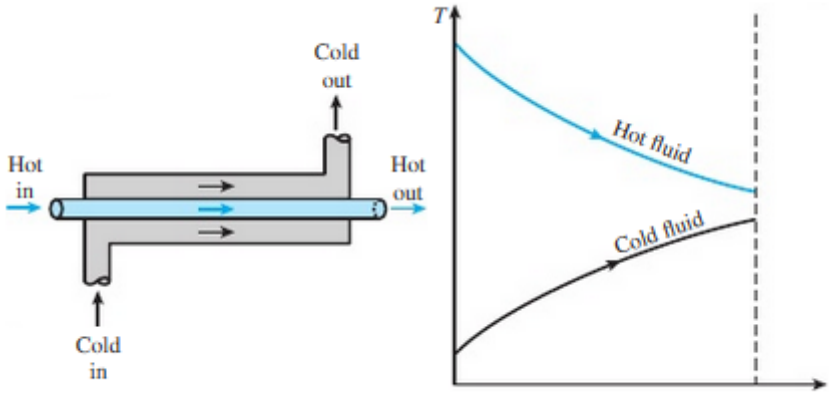

Figure 6 Parallel flow (Çengel & Ghajar, 2015)

3.2.2 Counter-flow

Counter-flow (Figure 7) heat exchangers are similar to parallel-flow heat exchangers, but instead of the fluids flowing in the same direction, they flow in the opposite direction to each other. Since the inlet of the hot fluid and the outlet of the same fluid are at the same end, the cooler fluid will approach the inlet temperature of the hot fluid. This means that the cold fluid can reach a higher temperature than the lowest temperature of the hot fluid. Due to this, the counter flow is the most efficient heat exchanger if maximum temperature increase or decrease is desired (U.S. Department of Energy, 1993).

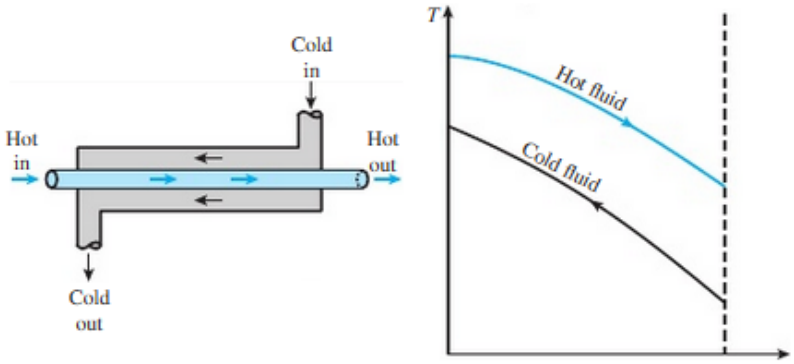

Figure 7 Counter flow (Çengel & Ghajar, 2015)

3.2.3 Cross-flow

In cross-flow (Figure 8) heat exchangers, the fluids flow perpendicular to each other. In other words, the fluid in the shell flows around the flow in the tubes at a 90° angle. They are usually used in applications where one of the fluids changes phase, for example a condenser where cooling water flows through the tubes absorbing heat from the steam flowing around the tubes condensing it into water (U.S. Department of Energy, 1993). Cross-flow heat exchangers can be either unmixed or mixed depending on the configuration.

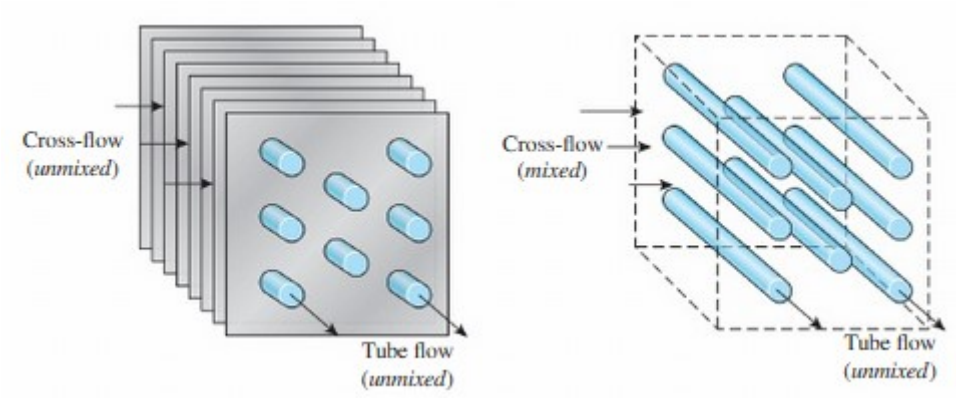

Figure 8 Cross flow a) Both fluids unmixed b) One fluid mixed, one fluid unmixed (Çengel & Ghajar, 2015)

3.3 Heat exchanger simulation

Modelling the dynamics of a heat exchanger can be done by using one of two general methods, distributed and lumped. They have different features which make them ideal for different applications (Varbanov, et al., 2011). The main features of the methods are compared in Table 1.

Table 1 Heat exchanger model type comparison (Varbanov, et al., 2011)

Property	Distributed model	Lumped model
Basic modelling element	Differential element	Heat exchange cell
Continuity	Continuous in both space and time	Continuous in time and discrete in space
Differentiation	Differential with regard to both space and time	Differential with regard to time only
Simplifying assumptions	Only two-stream heat exchangers are considered	Perfect mixing is assumed in the fluid compartments of each modelling cell
Solution methods	The approaches used vary from direct numerical integration using finite differences to hybrid methods using analytical solutions of the Laplace-transformed models and numerical approximation of the reverse Laplace transformation back into the time domain	Mostly direct numerical integration using finite differences, approximating the time derivatives. Note, that the physical space is already explicitly discretised by introducing the division of the exchanger into cells

Note: Reprinted from "Cell-based dynamic heat exchanger models—Direct determination of the cell number and size", by Varbanov, et al., 2011, *Computers & Chemical Engineering, 35,* p. 945.

General assumptions for dynamic heat exchanger models

I. Uniformly distributed heat transfer area throughout the heat exchanger.
II. All thermal properties except the stream temperatures are considered constant.
III. The heat conduction within the fluids and within the wall is considered negligible along the direction of the flow.
IV. The thermal resistance of the wall is neglected. This has the same effect as reducing the overall heat transfer coefficient and can be compensated by increasing the individual heat transfer coefficients.
V. No heat is lost to the surroundings (Varbanov, et al., 2011).

The distributed models use equations that are derived from the general differential equations for heat transfer in a material medium. The equations consider an infinitely small differential element of the wall or the fluid stream. The result is a model that consists of a few partial differential equations

with differentiation with respect to time and a spatial coordinate, such as length or height (Varbanov, et al., 2011).

Cell-based models are made by combining a number of perfectly mixed model tanks that are called cells. If the number of cells is large enough, the simulation results will be equivalent to those of the distributed model. Each heat exchange cell is expressed by two mass and three energy balances which are ordinary differential equations with respect to time (Varbanov, et al., 2011).

Both methods have their own advantages and disadvantages and are therefore generally used for different applications. Distributed models are usually preferred when investigating heat transfer dynamics in general or studying a heat exchanger in detail, since they recognise the continuous nature of the heat transfer, both in space and time. For studying complex heat exchangers or heat exchanger networks, it is generally preferred to use cell-based models. While the number of equations can become high, they are very simple and can be used for any type of heat exchanger. Another advantage of the cell-based model is that the complexity can easily be scaled by adjusting the number of cells (Varbanov, et al., 2011).

3.3.1 Heat exchange cell

Assumptions for cells

I. Perfect mixing in both tanks in each heat exchanger cell.
II. Constant fluid densities. This works well for liquids. For gases, this requires that the pressures are kept almost constant.
III. The tanks are completely filled with respective fluid.
IV. Since the aim of the heat exchanger model is to control the fluid temperatures, the flows are assumed to have constant specific heat capacities that are finite. This means that streams with pure vaporisation or condensation are excluded.
V. Due to the complex dynamics of heat transfer through the wall, the wall resistance to heat transfer is not taken into consideration. The temperature of the wall can then be assumed to be uniform within the cell volume. The heat capacity of the wall is, however, taken into account since the metal heating and heat buffering might cause a delay in heat flow and therefore influence the temperature distribution over time (Varbanov, et al., 2011).

Equations

In this section, the equations used in the heat exchangers are derived based on (Varbanov, et al., 2011), (Çengel & Ghajar, 2015) and (Häggblom, 2015).

The mass balance of a tank in a cell is

$$\frac{dM_{\mathrm{TANK}}}{dt} = \dot{m}_{\mathrm{in}} - \dot{m}_{\mathrm{out}}, \tag{1}$$

where $\dot{m}_{\mathrm{in}}$ and $\dot{m}_{\mathrm{out}}$ are the mass flows of the fluid and M_{TANK} is the mass of the fluid in the tank.

The energy balance is

$$\frac{dE_{\mathrm{TANK}}}{dt} = \dot{E}_{\mathrm{in}} - \dot{E}_{\mathrm{out}} \pm \dot{Q}_{\mathrm{CELL}}, \tag{2}$$

where $\dot{E}_{\mathrm{in}}$ and $\dot{E}_{\mathrm{out}}$ are the energy flows in and out of the tank and $\dot{Q}_{\mathrm{CELL}}$ is the heat transfer rate through the wall of the tank. The heat is added for the cold side and subtracted for the hot side of the tank.

The energy of a matter is proportional to its mass or mass flow and absolute temperature. This gives the constitutive equations

$$E = c_{\mathrm{p}} T_{\mathrm{out}} M_{\mathrm{TANK}}, \qquad \dot{E}_{\mathrm{in}} = c_{\mathrm{p}} T_{\mathrm{in}} \dot{m}_{\mathrm{in},}, \qquad \dot{E}_{\mathrm{out}} = c_{\mathrm{p}} T_{\mathrm{out}} \dot{m}_{\mathrm{out}}, \tag{3}$$

where c_{p} is the heat capacity of the fluid and T_{in} and T_{out} are the absolute temperatures of the fluid at the inlet and outlet of the tank.

Due to assumptions (II), (III) and (IV) in the list above eliminating changes in mass flows, specific heat capacity and fluid holdup, Equation (2) can now be written as

$$M_{\mathrm{TANK}} c_{\mathrm{p}} \frac{dT_{\mathrm{out}}}{dt} = \dot{m} c_{\mathrm{p}} T_{\mathrm{in}} - \dot{m} c_{\mathrm{p}} T_{\mathrm{out}} \pm \dot{Q}_{\mathrm{CELL}}. \tag{4}$$

The heat transfer rate of the hot and the cold tanks are given by

$$\dot{Q}_{\mathrm{CELL,H}} = K_{\mathrm{H}}\left(T_{\mathrm{H,out}} - T_{\mathrm{w}}\right), \tag{5}$$

$$\dot{Q}_{\mathrm{CELL,C}} = K_{\mathrm{C}}\left(T_{\mathrm{w}} - T_{\mathrm{C,out}}\right), \tag{6}$$

with $K = h(t)A$, where h is the heat transfer coefficient and A is the heat transfer area in a cell. T_w is the absolute temperature of the wall between the tanks.

Due to assumption (V), the energy balance of the wall is

$$\frac{dE_{\mathrm{w}}}{dt} = \dot{Q}_{\mathrm{CELL,H}} - \dot{Q}_{\mathrm{CELL,C}}. \tag{7}$$

Using Equations (5) and (6), Equation (7) can be transformed into

$$\frac{dE_{\mathrm{w}}}{dt} = K_{\mathrm{H}}\left(T_{\mathrm{H,out}} - T_{\mathrm{w}}\right) - K_{\mathrm{C}}\left(T_{\mathrm{w}} - T_{\mathrm{C,out}}\right). \tag{8}$$

Since the mass of the wall is clearly constant and by assuming the specific heat transfer is also constant, Equation (8) can be rewritten as

$$M_{\text{Steel}}\, c_{\text{p,Steel}} \frac{dT_{\text{w}}}{dt} = K_{\text{H}}\left(T_{\text{H,out}} - T_{\text{w}}\right) - K_{\text{C}}\left(T_{\text{w}} - T_{\text{C,out}}\right), \tag{9}$$

where M_{Steel} is the mass of the wall and $c_{\text{p,Steel}}$ is the specific heat capacity of the wall.

The heat transfer of a cell i in the heat exchanger model is described by the following differential equations transformed from Equations (4), (5), (6) and (9):

$$\frac{dT_{\text{H,out}}^{(i)}(t)}{dt} = \frac{\dot{m}_{\text{H}}(t)}{M_{\text{H}}}\left(T_{\text{H,in}}^{(i)}(t) - T_{\text{H,out}}^{(i)}(t)\right) - \frac{K_{\text{H}}}{M_{\text{H}} c_{\text{p,H}}}\left(T_{\text{H,out}}^{(i)}(t) - T_{\text{w}}^{(i)}(t)\right), \tag{10}$$

$$\frac{dT_{\text{C,out}}^{(i)}(t)}{dt} = \frac{\dot{m}_{\text{C}}(t)}{M_{C}}\left(T_{\text{C,in}}^{(i)}(t) - T_{\text{C,out}}^{(i)}(t)\right) + \frac{K_{\text{C}}}{M_{\text{C}} c_{\text{p,C}}}\left(T_{\text{w}}^{(i)}(t) - T_{\text{C,out}}^{(i)}(t)\right), \tag{11}$$

$$\frac{dT_{\text{w}}^{(i)}(t)}{dt} = \frac{K_{\text{H}}}{M_{\text{Steel}} c_{\text{p,Steel}}}\left(T_{\text{H,out}}^{(i)}(t) - T_{\text{w}}^{(i)}(t)\right) - \frac{K_{\text{C}}}{M_{\text{Steel}} c_{\text{p,Steel}}}\left(T_{\text{w}}^{(i)}(t) - T_{\text{C,out}}^{(i)}(t)\right), \tag{12}$$

where $c_{\text{p,C}}$ and $c_{\text{p,H}}$ are the specific heat capacities of the cold and hot side respectively. M_{H} and M_{C} are the masses of the fluids at the hot and cold side.

If the wall is ignored, Equations (13)-(15) replace Equations (5), (6) and (10)-(12).

$$\dot{Q}_{\text{CELL}} = K\left(T_{\text{H,out}} - T_{\text{C,out}}\right), \tag{13}$$

$$\frac{dT_{\text{H,out}}^{(i)}(t)}{dt} = \frac{\dot{m}_{\text{H}}(t)}{M_{\text{H}}}\left(T_{\text{H,in}}^{(i)}(t) - T_{\text{H,out}}^{(i)}(t)\right) - \frac{K}{M_{\text{H}} c_{\text{p,H}}}\left(T_{\text{H,out}}^{(i)}(t) - T_{\text{C,out}}^{(i)}(t)\right), \tag{14}$$

$$\frac{dT_{\text{C,out}}^{(i)}(t)}{dt} = \frac{\dot{m}_{\text{C}}(t)}{M_{\text{C}}}\left(T_{\text{C,in}}^{(i)}(t) - T_{\text{C,out}}^{(i)}(t)\right) + \frac{K}{M_{\text{C}} c_{\text{p,C}}}\left(T_{\text{H,out}}^{(i)}(t) - T_{\text{C,out}}^{(i)}(t)\right), \tag{15}$$

Figure 9 shows how the heat exchanger in the model is constructed.

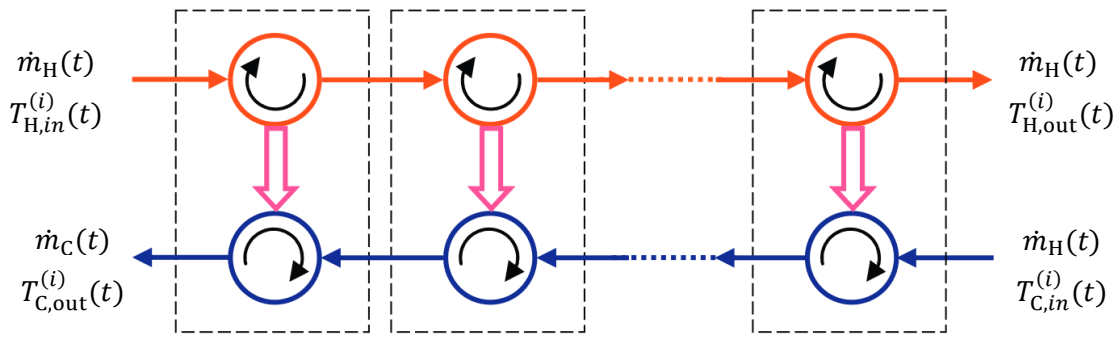

Figure 9 Cell arrangement of a single-pass shell-and-tube heat exchanger (Varbanov, et al., 2011)

In Figure 10, a heat exchanger cell which includes the wall is shown.

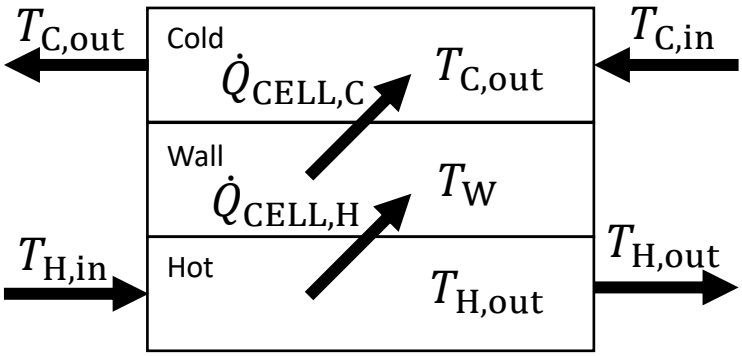

Figure 10 Heat exchanger cell including the wall

3.3.2 Driving forces

The driving force for heat transfer in heat exchangers is temperature difference. In the cell model, the driving force is estimated using the temperature difference between the cells. This temperature difference is smaller than the real temperature differences of the heat exchanger. This effect is strong when the number of cells is small, but becomes weaker the more the number of cells increases. The heat transfer coefficient in cell models has to compensate for this and is, therefore, larger than it would be for an actual heat exchanger (Varbanov, et al., 2011) as shown in Figure 11. This is included in the simulation by changing K in Equations 10, 11 and 12 into $K = XhA$ where X is a positive number.

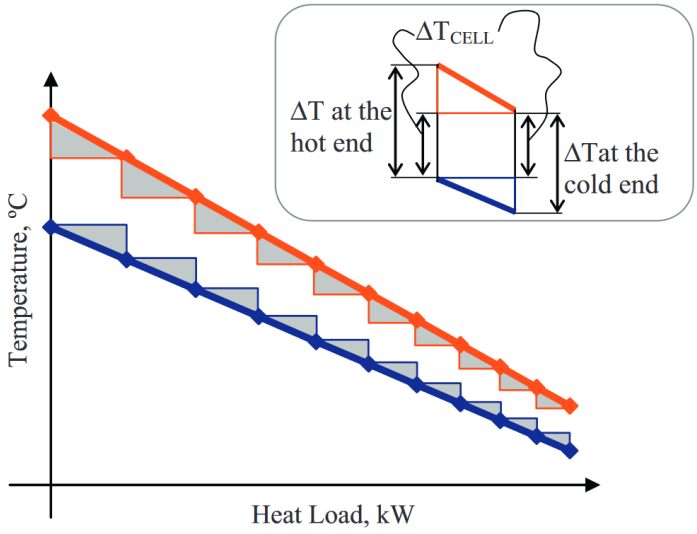

Figure 11 Driving forces are lower in the cell model

3.3.3 Determining the minimum number of cells

There are a number of ways to determine the minimum number of cells needed for adequate simulation of a heat exchanger.

The specifications of one of the heat exchangers in the engine cooling system was made available for use in the thesis. These values are listed in Table 2 and were used in the examples.

Table 2 Heat exchanger specification

Property	Cold flow	Hot flow
Specific heat capacity (J/(kg*K))	4190	4190
Mass flow (kg/s)	46.22	56.27
Inlet temperature (°C)	68	91
Desired outlet temperature (°C)	88.6	74.1

Graphical method in (Varbanov, et al., 2011)

If the number of cells is reduced below a certain number, the temperature differences become negative, which would make the model thermodynamically incorrect. This creates a limiting case if zero temperature difference is assumed in all cells of the heat exchanger. This was used by (Varbanov, et al., 2011) to create a graphical method based on McCabe & Thiele's (1925) method to determine the number of stages needed to calculate a binary distillation column. This is drawn as a series of steps that starts from one end of the heat exchanger as shown in Figure 12. The temperature curves are straight lines drawn between respective inlet and outlet temperature.

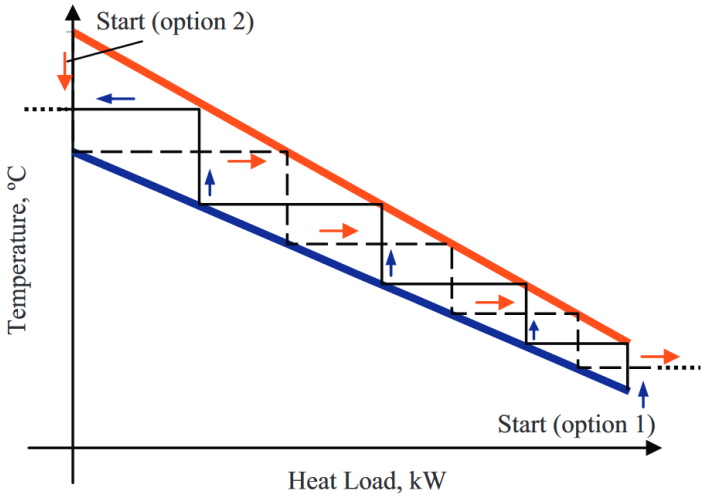

Figure 12 Minimum number of cells based on the difference in temperature

It does not matter at which end of the heat exchanger the procedure is started, but in this example, option 1 is used. First, a vertical line is drawn from the cold flow to the hot flow at the cold end of the heat exchanger, then a horizontal line is drawn leftwards from that point until it reaches the cold flow, which marks the end of the first cell. The same procedure is used to draw the rest of the cells until the horizontal line exits at or above the cold water temperature at the hot end of the heat exchanger. In this example, the minimum number of steps is four. This can also be done in the opposite direction using option 2, which results in the same number of cells as option 1.

The method in Figure 12 works by assuming that the heat transfer coefficient of the cells is very large (infinite). As a result of this, the cold temperature out of the cell will be the same as the hot temperature into the cell, which means a straight line can be drawn. By then stepping as the method proposes, the lower limit of the number of steps needed to be able to find a finite K such that the temperatures out of the heat exchanger is the same as in the specification can be found. An important note is that this method does not say anything about how many cells that should be used, only the minimum number of cells required to find a finite K.

Using the values in Table 2, this method was done in two slightly different ways using different graphs. The left graph in Figure 13 approximates the temperature profile with straight lines like Varbanov, while the right graph uses the method described in Section 3.3.4 with $n = 100$. The result of both versions is that a minimum of five cells is needed.

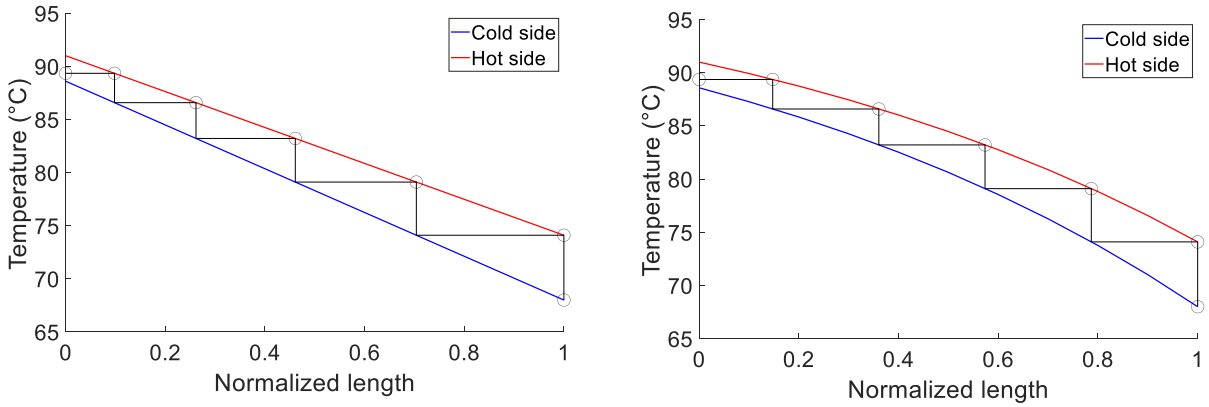

Figure 13 Left) Straight lines Right) Calculated curves

Simulink model

Another way to determine the minimum number of cells needed to simulate a heat exchanger is by using simulation software, for example Simulink, which is the software used in this thesis. This was done using two models, one model which included the wall while the other model ignored the wall. The first one is based on Equations (10)-(12) while the other uses Equations (13) and (14). The following procedure was used in the thesis:

Step 1. Initialise the design parameters with one cell.

Step 2. Set h to a very large number.

Step 3. Run the simulation.

Step 4. If the simulated outlet temperature of the cold flow exceeds the desired temperature, the minimum number of cells has been found. If not, increase the number of cells by one and repeat from Step 3.

Using the values in Table 2, both versions required a minimum of five cells to fulfil the requirement of Step 4.

Since all methods listed in this section give the same result, it can be concluded that the minimum number of cells required for the heat exchanger in Table 2 is five.

3.3.4 Adapting the heat exchanger model to design specifications

In practice it would be useful to have a method for determining the cell heat transfer coefficient of the model such that the outlet temperatures match the design specifications of the physical heat exchanger. For this purpose, a steady-state analysis is sufficient.

The steady-state energy balances are obtained from Equations (13)-(15) by setting the derivatives to zero. In this analysis the effect of the cell wall is ignored by assuming that $T_w^{(i)}(t) = T_{C,out}^{(i)}(t)$ as $t \to \infty$. For simplicity's sake, the heat transfer is assumed to be $K = K_{\mathrm{C}} = K_{\mathrm{H}}$. For the sake of notational clarity, the steady-state outlet temperatures are denoted as $T_{\mathrm{C}}(i)$ and $T_{\mathrm{H}}(i)$ on the cold and hot sides respectively for cells $i = 1,2,\dots,n$. The steady-state relations are then given by the linear system of equations

$$
\begin{aligned}
&(c_{p,C}\dot{m}_C + K)T_C(1) - KT_H(n) = c_{p,C}\dot{m}_C T_{C,in}\\
&(c_{p,C}\dot{m}_C + K)T_C(2) - c_{p,C}\dot{m}_C T_C(1) - KT_H(n-1) = 0\\
&\vdots\\
&(c_{p,C}\dot{m}_C + K)T_C(n) - c_{p,C}\dot{m}_C T_C(n-1) - KT_H(1) = 0\\
&(c_{p,H}\dot{m}_H + K)T_H(1) - KT_C(n) = c_{p,H}\dot{m}_H T_{H,in}\\
&(c_{p,H}\dot{m}_H + K)T_H(2) - c_{p,H}\dot{m}_H T_H(1) - KT_C(n-1) = 0\\
&\vdots\\
&(c_{p,H}\dot{m}_H + K)T_H(n) - c_{p,H}\dot{m}_H T_H(n-1) - KT_C(1) = 0.
\end{aligned}
\tag{16}
$$

Given the heat exchanger parameters, inlet temperatures and mass flows, equation system (16) can be expressed in a matrix form

$$A(K)x = b, \tag{17}$$

where $A(K)$ is a $2n$-by-$2n$ matrix that depends on the unknown variable K and the heat exchanger parameters The vector x is defined as $x = [T_C(1) \quad \cdots \quad T_C(n) \quad T_H(1) \quad \cdots \quad T_H(n)]^T$ and $b = [c_{p,C}\dot{m}_C T_{C,in} \quad 0 \quad \cdots \quad c_{p,H}\dot{m}_H T_{H,in} \quad 0 \quad \cdots]^T$. Assuming that $A(K)$ is invertible for all K, the outlet temperatures x are given by

$$x = [A(K)]^{-1}b. \tag{18}$$

Defining a vector $y = [T_{C,out} \quad T_{H,out}]^T$, where $T_{C,out}$ and $T_{H,out}$ are the desired outlet temperatures, and a 2-by-$2n$ matrix C such that

$$y = Cx = C[A(K)]^{-1}b, \tag{19}$$

the parameter K which results in the model that best fits the design specifications is obtained by minimising the cost function

$$J(K) = \|y - Cx\|_2^2 = \|y - C[A(K)]^{-1}b\|_2^2, \tag{P1}$$

where $\|\cdot\|_2$ denotes the ℓ_2 vector norm. Although this is a non-convex problem with respect to K, since the only unknown parameter is scalar, optimisation problem (P1) can either be solved by trial-and-error or by using the unconstrained optimisation solver `fminunc()` in MATLAB. Note that for a small number of cells n, the obtained K might be very large and it would be advantageous to use a larger n than the minimum number of cells obtained by the graphical method presented in Section 3.3.3.

The proposed method can be summarised as follows:

Step 1. Initialise the design parameters $c_{p,C}, c_{p,H}, \dot{m}_C, \dot{m}_H, T_{C,in}, T_{H,in}, T_{C,out}, T_{H,out}$ according to the heat exchanger specifications.

Step 2. Determine the number of cells n needed using the graphical method presented in Section 3.3.3.

Step 3. Solve optimisation problem P1 to obtain the needed K.

Step 4. Divide K by A/n to obtain the cell heat transfer coefficient h_{CELL}. X mentioned in Section 3.3.2 can be obtained if h_{CELL} is divided by h.

Since this method was developed at a late stage of the project, after the adaption of the engine cooling system, manual tuning using hX was instead done directly in Simulink. Table 3 shows the X values of the manual adaption compared to the MATLAB code using h in Table 2 and an assumed heat exchanger area of $120\ m^2$. The "no walls" difference is mostly due to slightly different optimisation objectives. The MATLAB code minimises the temperature errors while the manual method tried to make the outlet temperature of the cold flow reach the desired temperature.

The reason why the X values when the wall is taken into account are twice as high as the values when the wall is ignored can be explained by using Equations (5), (6), and (13). Since perfect mixing is assumed (assumption (I) in Section 3.3.1), the water temperature in steady-state (in a cell) is $T_{\mathrm{C,out}}$ at

the cold side and $T_{\mathrm{H,out}}$ at the hot side and the wall temperature is $T_W = \frac{T_{\mathrm{H}}+T_{\mathrm{C}}}{2}$. This can then be combined with Equation (5) to describe the heat transfer rate from the hot side to the wall:

$$\dot{Q}_{\mathrm{CELL,H}} = K\left(T_{\mathrm{H,out}} - T_{\mathrm{W}}\right) = K\left(T_{\mathrm{H,out}} - \frac{1}{2}\left(T_{\mathrm{H,out}} + T_{\mathrm{C,out}}\right)\right) = \frac{K}{2}\left(T_{\mathrm{H,out}} - T_{\mathrm{C,out}}\right), \quad (20)$$

and with Equation (6) to describe the heat transfer rate from the wall to the cold side:

$$\dot{Q}_{\mathrm{CELL,C}} = K\left(T_{\mathrm{W}} - T_{\mathrm{C,out}}\right) = K\left(\frac{1}{2}\left(T_{\mathrm{H,out}} + T_{\mathrm{C,out}}\right) - T_{\mathrm{C,out}}\right) = \frac{K}{2}\left(T_{\mathrm{H,out}} - T_{\mathrm{C,out}}\right). \quad (21)$$

Since both equations result in a $\dot{Q}$ value that is half of that in Equation (13), it explains why the X value (or the cell heat transfer coefficient, h_{CELL}) when the wall is taken into account has to be twice that of the value when the wall is ignored.

Table 3 Comparison between Simulink and MATLAB

Number of cells	X (Simulink (no walls))	X (MATLAB (no walls))	X (Simulink (walls))
5	19	17.7700	38
7	3.2	3.1546	6.4
8	2.53	2.5090	5.06
20	1.355	1.3483	2.71
32	1.215	1.2084	2.43
64	1.115	1.1122	2.23

While five cells are enough for the simulation, it was decided to use eight cells in the model. This was done to have a margin of error during simulation.

4 Cooling water systems

4.1 Freshwater cooling systems

Large marine diesel engines are usually water-cooled, and so are all four engines in the reference ship. About 25% of the chemical energy in the fuel is transformed into heat and has to be removed from the engine. This is done by having a closed freshwater cooling system for each engine, which is split into two separate circuits: a high-temperature (HT) and a low-temperature (LT) circuit. The freshwater system is cooled in a central cooler using an open seawater cooling system. Figure 14 shows a simplified version of the engine cooling system of one of the engines on the reference ship.

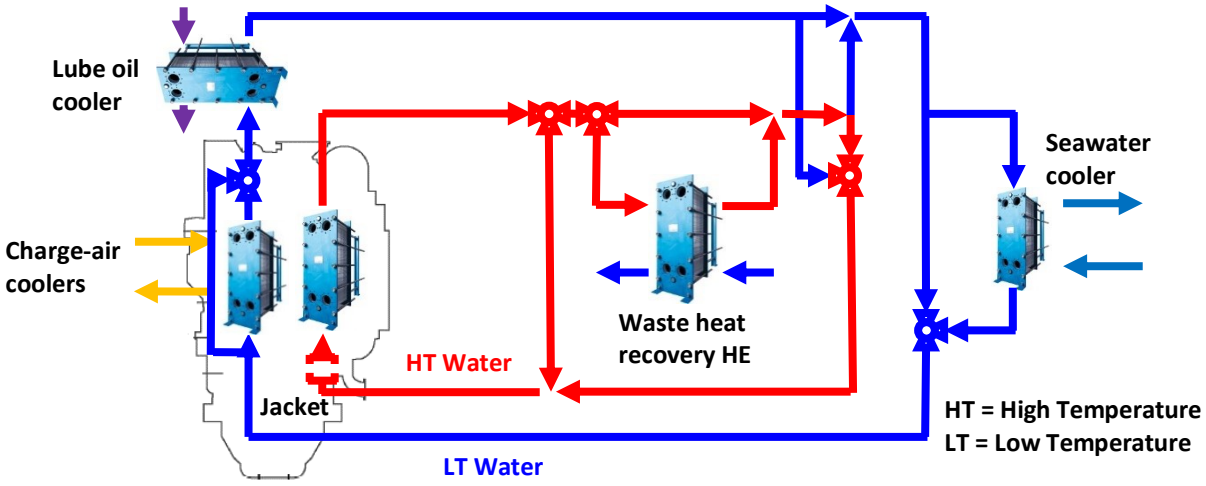

Figure 14 Simplified engine cooling system (Manngård, 2019), modified by the author

4.1.1 HT circuit

The HT circuit is used to cool the cylinder liner, the cylinder head and the first stage of the charge air cooler. The cooling water is pumped by an engine-driven pump mounted at the free end of the engine. Since the engine is run at a constant speed, the HT water flow is constant. After the charge air cooler the water flows to a thermostatic valve that controls how much is sent to the waste heat recovery (WHR) heat exchanger respective circulated directly back into the engine. The HT water is cooled by mixing with LT water using a valve.

4.1.2 LT circuit

The LT circuit cools the second stage of the charge air cooler and the lube oil cooler. The LT pump is electrically driven with a constant flow rate. One of the tasks of the LT water is to cool charge air to a constant temperature at the engine inlet. This is controlled by letting some of the flow bypass the charge air cooler. The LT water is cooled with seawater in the central cooler.

4.2 Seawater cooling system

To get rid of excess heat energy from the freshwater circuits, an open seawater circuit is used to dump heat into the sea. Seawater is pumped from the sea through the central cooler where heat from the LT circuit is transferred to the seawater and then led back into the sea. The main method of controlling the LT water temperature is by controlling the pump power. If the LT water is still too cold, a valve will open to let some of the water bypass the cooler.

5 Control system

The initial model had a control system consisting of five PI controllers, one for each of the five valves that are controlled by the automation system. This control system was updated when specifications of the real control of the reference ship where made available.

5.1 3-way valves

3-way valves are used to control the temperature of a flow. This can be done with either mixing or diverting valves. If placed at the supply (before the application), a diverting valve is used. If placed at the return (after the application), a mixing valve is used. Diverting valves are usually more expensive than mixing valves.

On the reference ship, all 3-way valves in the engine cooling system and the WHR system are mixing valves except the one immediately after the HT charge air cooler. In the model, however, diverting valves are used instead. This is due to how Simulink works. It uses signals instead of physical properties like flow rate and temperature. This means that the flow has to be calculated before the heat exchanger. Figure 15 shows the placement of the 3-way valves in the engine cooling system. The valves are (1) heat recovery, (2) central cooler, (3) second stage of the charge air cooler, (4) lube oil cooler, (5) HT water at engine outlet, and (6) WHR. T1-5 are temperature sensors and PI1-5 are PI-controllers.

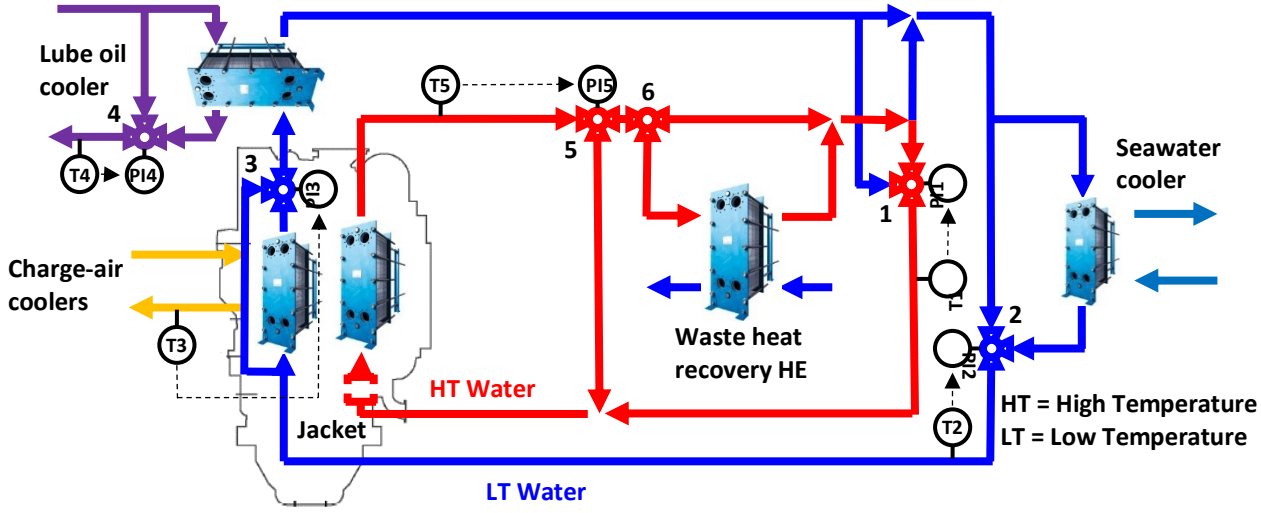

Figure 15 Simplified engine cooling system with valves, sensors and PI-controllers (Manngård, 2019), modified by the author

5.1.1 Temperature control valve for heat recovery

Valve 1 is used to control the maximum temperature of the water that is mixed with HT water from the engine outlet before the HT pump. The temperature is controlled using a mixing valve where HT water and LT water is mixed to keep the HT temperature constant at a certain setpoint depending on engine load (Engine manufacturer, 2019).

5.1.2 Temperature control valve for central cooler

Valve 2 controls the LT water temperature before the engine by letting some of the water bypass the cooler. The valve is used only when the seawater pump is at its lowest speed and the LT water is still too cold. The LT water temperature setpoint is variable and depends on engine load (Engine manufacturer, 2019).

5.1.3 Temperature control valve for the second stage of the charge air cooler

Valve 3 controls the charge air temperature at the engine inlet by partially bypassing LT water. Thus, a constant charge air temperature can be maintained at the inlet.

5.1.4 Temperature control valve for lube oil cooler

Valve 4 controls the lube oil temperature at the engine inlet by partially bypassing lube oil. This keeps the lube oil temperature at the inlet constant.

5.1.5 Temperature control valve for HT water at the engine outlet

Valve 5 controls the HT water temperature at the engine outlet. This is used to keep the outlet temperature at a certain setpoint depending on load and seawater temperature.

5.1.6 WHR valve

Valve 6 controls the flow to the WHR heat exchanger. It is manually controlled and is used only when the WHR heat exchanger is undergoing maintenance by letting the flow fully bypass it. Under normal conditions, it sends everything through the heat exchanger.

6 Simulation tool

Process simulation describes industrial processes by means of the application of first principles (e.g. conservation laws and thermodynamics) and mathematics (e.g. differential equations). There are two different types of process simulation, steady state and dynamic. The main difference between them is that steady state assumes that variables are constant and does not consider the effects of time. Dynamic simulation, by contrast, does consider the effects of time and assumes that the model is in a state of change (da Silva, 2015). Dynamic simulation is the most suitable method for creating an engine cooling system digital twin due to the ship and its surroundings being in a constant state of change.

There is a large variety of applications that require dynamic simulation software. Some software are made for more specific applications while others are made for more general use. Some examples of dynamic simulation software for more specialised use are Apros Thermal and FreeDyn. Apros Thermal is specialised for thermal power plants while FreeDyn is designed for multibody dynamics (Fortum Heat and Power, 2019; FreeDyn, 2019). Simulink and Xcos, by contrast, are more general tools (MathWorks, 2019; Scilab, 2019).

6.1 Simulink

Simulink is a system dynamics software. It was chosen for the modelling of the digital twin since it is a standard tool used both in the industry and for research.

7 Navigating large datasets

The first part of the thesis work was to analyse and sort out data from a large dataset provided by the shipyard as an Excel spreadsheet. A separate Excel spreadsheet with descriptions was also provided which helped considerably when trying to determine what the sensors actually measured.

7.1 Description of the data

The data was taken from a modern cruise ship during 31 days in March/April 2018. The dataset consisted of 566 sensors in total reported as one-minute averages, a total of 44 640 rows per column.

7.2 Sorting out data

The data was analysed to try and learn why certain things were happening on the reference ship during those days. For example, plotting the seawater temperature showed that it was quite stable at 27 °C for days before it suddenly started to drop with a relatively constant speed until it stabilised at about 15 °C at the end of the data. The seawater temperature also had strange intervals where the temperature rose slowly until suddenly dropped. Figure 16 shows the seawater temperature during the 31-day trip.

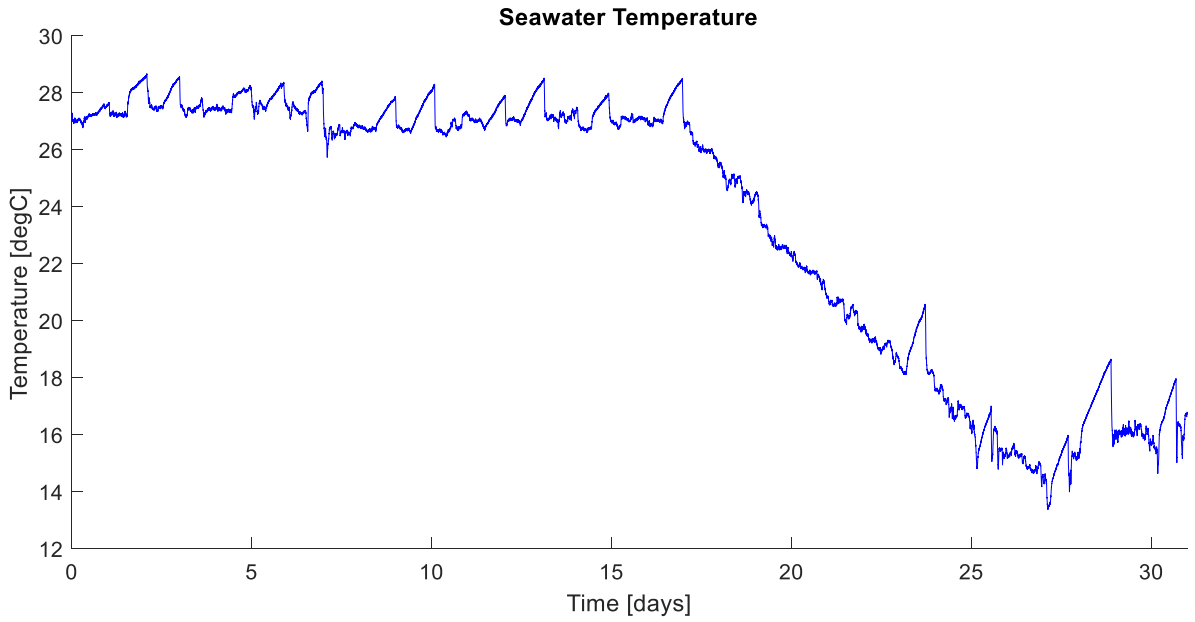

Figure 16 Seawater temperature

To solve this, the latitude and longitude coordinates were added to 3D Maps in Microsoft Excel so that the itinerary of the reference ship could be determined. This showed that the cruise ship was in the Caribbean during the first 17 days, then undertook a six-day crossing of the Atlantic heading northeast, then spent six days in the Mediterranean Sea before starting to cross the Atlantic again, presumably

to the Caribbean. The intervals with increased temperature occur in the harbour since the used cooling water heats up the seawater close to the sensor.

The 3D Map was also used to determine when the different engines are in use. For example, in port only one of the two smaller engines is online at about 50% load. However, one of the larger engines is almost always in use when not in port. This is the engine that was used as the base for the simulation of the engine cooling system due to the larger amount of data relevant to the thesis.

Since the model in Chapter 8 only uses static inputs, the next step was to analyse the data to determine which sensors were needed to run dynamic simulations of the engine cooling system and which ones could be used to adapt and validate it. The sensors used for simulation input were found by checking the initial model of the system and then trying to determine the signal name in the spreadsheet. The five inputs that were found are listed in Table 4.

Table 4 Inputs used in the engine cooling simulation

Input	Description	Unit	Notes
DG x power	Power for Diesel Generator x	kW	Changed to load in simulation
DG x compressor intake air temperature	Air temperature at the turbo compressor intake for Diesel Generator x	°C	
Seawater temperature	Seawater temperature	°C	
WHR flow rate	Flow rate of the secondary flow through the WHR heat exchanger	kg/s	Rough estimation based on the total flow rate The sensor reports the flow rate in m3/h
WHR temperature	Temperature of the secondary flow through the WHR heat exchanger	°C	The closest sensor was faulty, so the next one further back was used

The sensors used for validation are T1, T2 and T5 shown in Figure 15. T1 is referred to as “LT Water”, T2 as “HT Water In” and T5 as “HT Water Out” in the figures from now on.

8 Digital twin

8.1 Initial model of the engine cooling system

A basic model of the engine cooling system made by (Manngård, et al., 2019) was provided for use in the thesis. This meant that focus could be put on adapting the model to data instead of creating a model. Figure 17 shows the basic model.

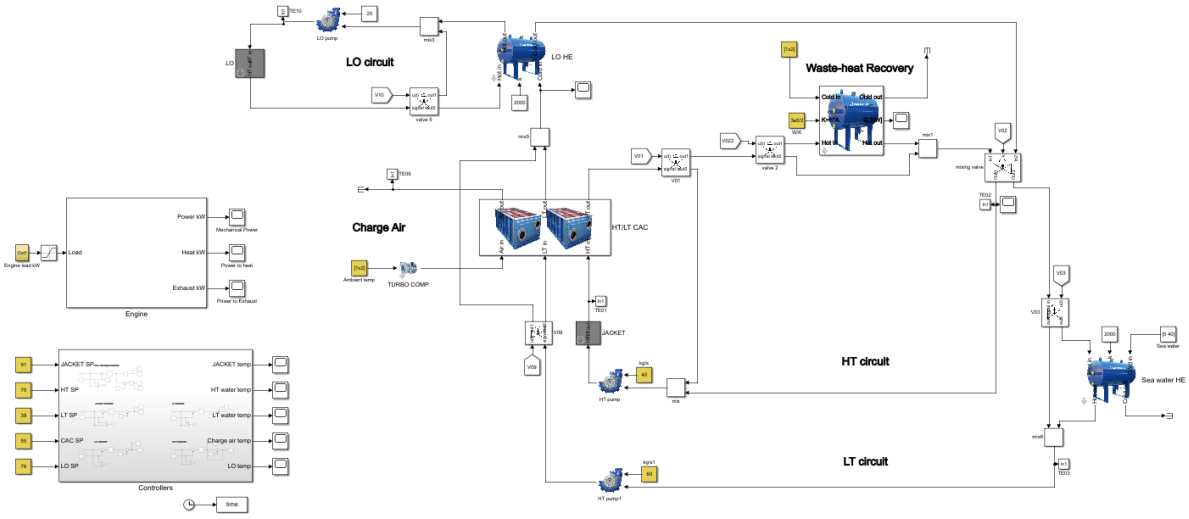

Figure 17 Base version of the engine cooling system model

8.2 Adapting the model

The reference ship has four engines of the same cylinder bore, but different number of cylinders. This meant that one engine could be the focus while adapting the model, whereas the rest could easily be modified in the end using the first engine as the base. Engine number 1 (DG1) was chosen to be the main focus since it was the engine most in use during the time the data was collected.

8.2.1 Updating parameters

The first step was to update parameters using the engine product guide and asking an employee at the shipyard for information. Flow rates and temperatures in the base model were qualified guesses while the setpoints for the temperature control valves (TCV) were taken from the product guide. The setpoints will be discussed later. The following constant parameters were updated:

- HT circuit flow rate
- LT circuit flow rate
- LO circuit flow rate
- Amount of water in the WHR heat exchanger

The charge air flow rate and temperature, WHR flow rate and temperature and seawater temperature were also changed, but were later made dynamic. A special case, the seawater flow rate, was also changed to better match the flow rate at maximum load. This flow rate should be dynamic, but due to the lack of pump information, a 3-way valve in the LT circuit handles the cooling power of the seawater heat exchanger instead.

8.2.2 Adding real data as inputs

After the parameters were updated, the following step was to start making the model dynamic by using sensor data provided by the shipyard. The first set of data to be added was the mechanical engine power. At the same time, the energy distribution of the fuel energy was updated according to the engine product guide, as shown in Figure 18 and Figure 19. This revision was later found to have a problem and had to be updated again, which will be discussed later. The setpoints were also slightly changed due to the data.

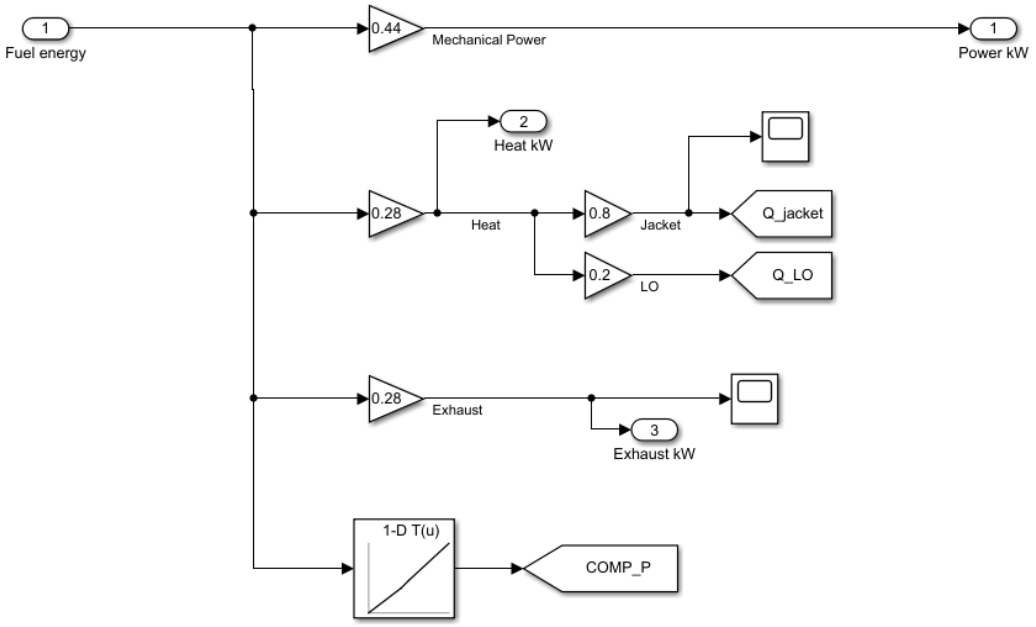

Figure 18 Base version of the energy distribution of the marine diesel engine

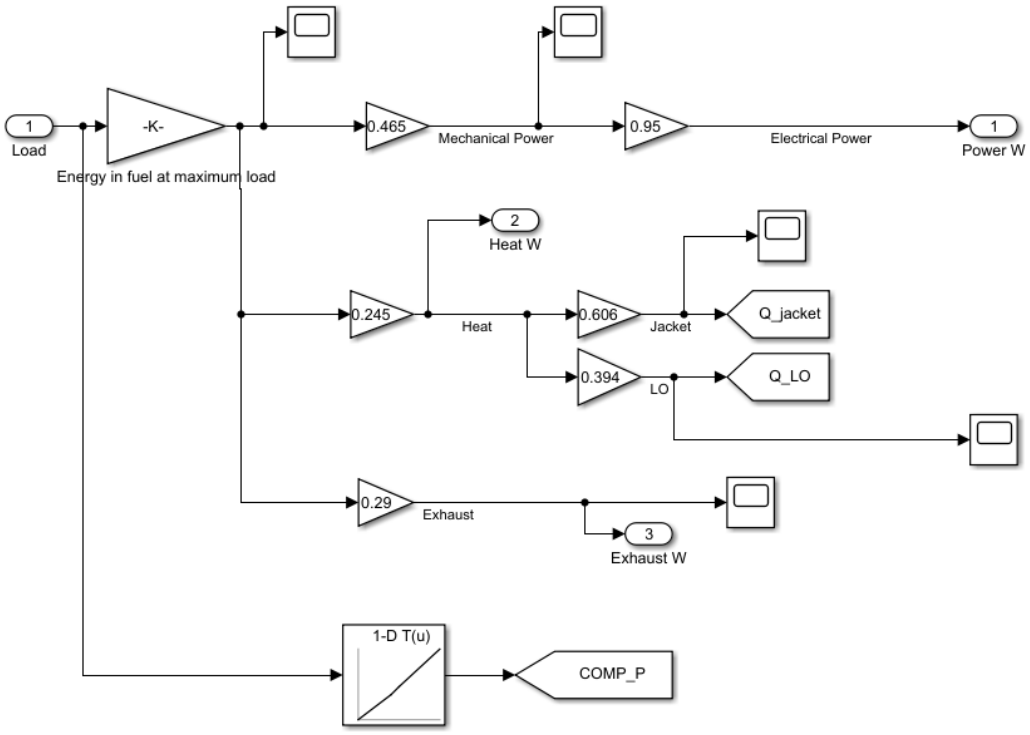

Figure 19 First revision of the energy distribution of the marine diesel engine

The next sensor data to be added was the charge air temperature at the turbine inlet and the seawater temperature. Especially the seawater temperature had a large effect on the simulation results. Comparing Figure 20 and Figure 21, it is clear that the seawater temperature is an important parameter in the modelling of the system.

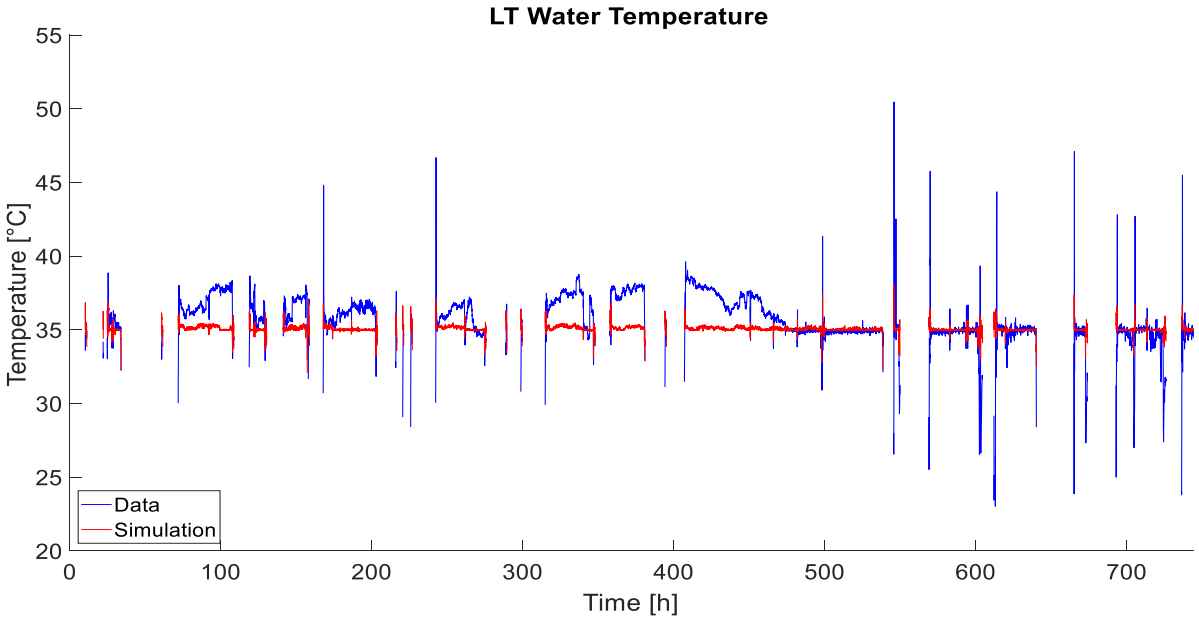

Figure 20 LT temperature after the seawater heat exchanger with a constant seawater temperature of 25 °C (data when the engine is offline has been excluded)

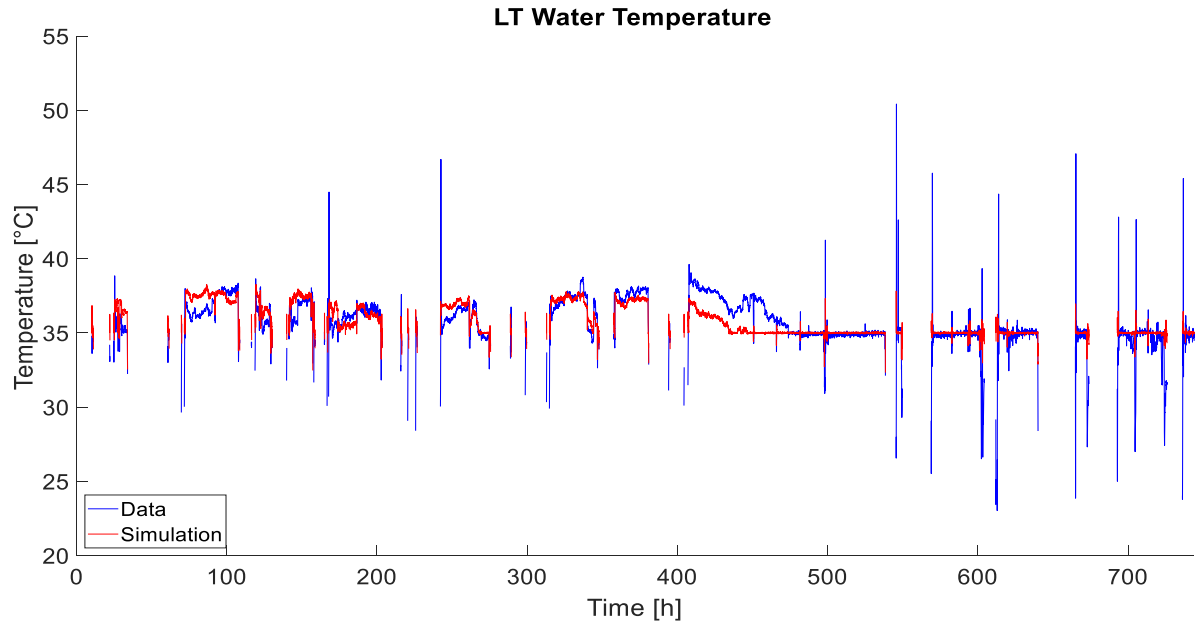

Figure 21 LT temperature after the seawater heat exchanger with the seawater temperature taken from data (data when the engine is offline has been excluded)

The next step was to make the charge air flow dynamic using data from the product guide and slightly change the lookup table for the turbo compressor ratio. The WHR flow rate was also changed to use data instead of a constant. This, however, is only a rough approximation using average flows that depends on different factors due to the lack of flowmeters in the flows to the WHR heat exchangers.

8.2.3 Sensor location

Until this point, it was thought that the sensor for the HT temperature after the engine was placed between the engine jacket and the second stage of the charge air cooler. This fit the data well although

the temperature after the charge air cooler seemed too high, as it reached about 100 °C. After looking more closely at the engine product guide and consulting an employee at the shipyard, it was confirmed that the sensor is actually placed after the charge air cooler.

This realisation caused some problems, since it meant the temperature after the charge air cooler that was now reaching 100 °C was supposed to be several degrees lower. Figure 22 shows the large temperature difference between data and simulation. The temperatures are very close at a few intervals when the engine has a lower load, but mostly the difference is about 6 °C.

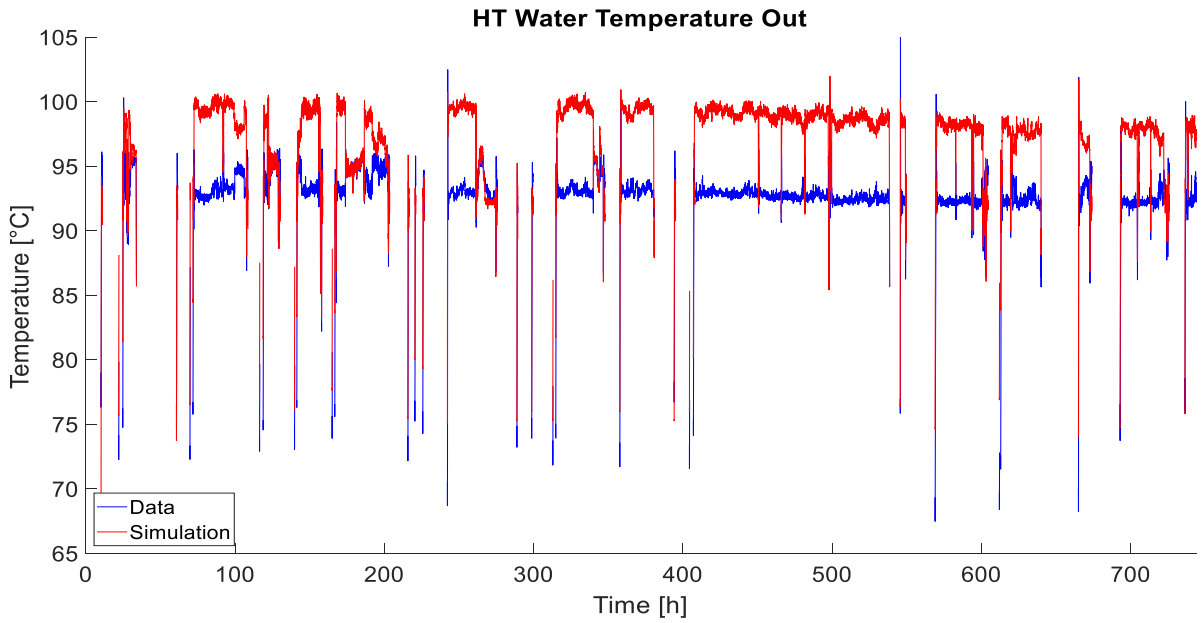

Figure 22 HT temperature after the charge air cooler (data when the engine is offline has been excluded)

This made it clear that too much heat was being transferred from the jacket to the HT water. However, no logical reason could be found, since the energy distribution was thought to be correct. Instead, work shifted to the heat exchangers, since simulations showed that a two-cell model was not enough to simulate realistic temperatures. The WHR heat exchanger and the seawater heat exchanger were the first to be changed to an eight-cell model. Some faulty parameters in the LO subsystem were also changed to more closely match reality. After the modification, the simulation temperatures decreased by about 2 °C (Figure 23). Compared to the data the difference was now about 4 °C.

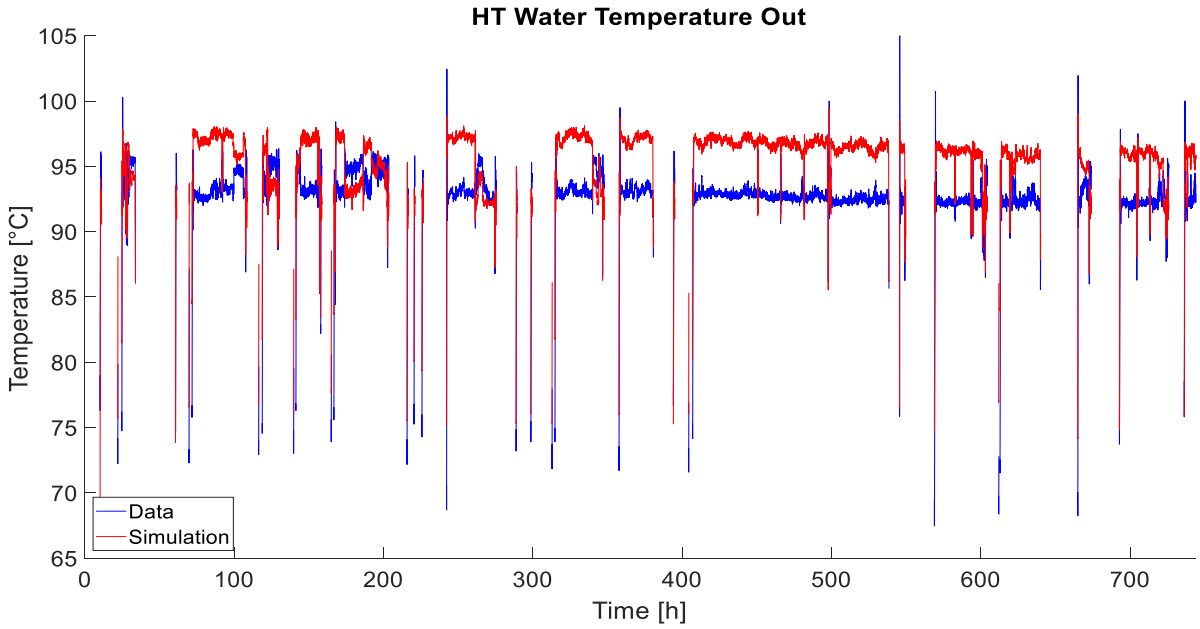

Figure 23 HT temperature after the charge air cooler (data when the engine is offline has been excluded)

Next, an error with the energy distribution percentages was found; too much heat was added to the HT circuit and the LT circuit. This was caused by having the heat from the charge air transferred to respective circuit twice, both from the jacket or lube oil and the charge air coolers. As shown in Figure 24, this was changed so that the charge air heat does not enter the jacket or lube oil.

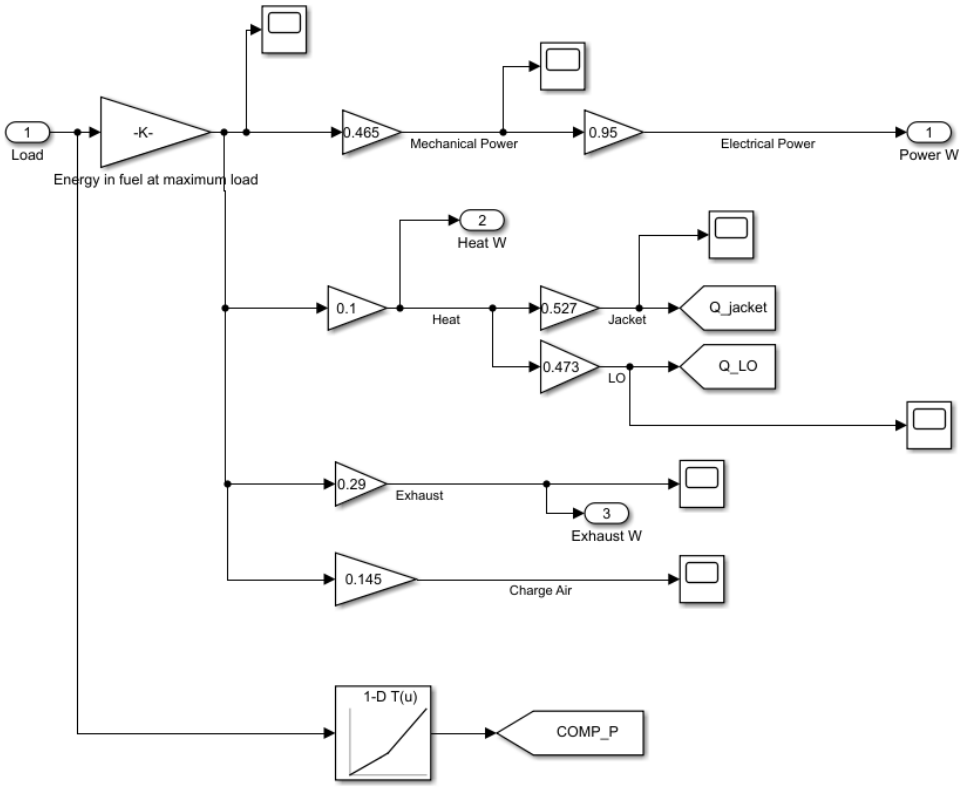

Figure 24 Second revision of the energy distribution of the marine diesel engine

Figure 25 shows that the simulation is now able to reach the real temperatures from the data. The next step was now to change the remaining two-cell heat exchangers to eight-cell ones, tune all heat exchangers and find the setpoints for the controllers. The WHR valve was also changed to let everything flow through the WHR heat exchanger to match the real system.

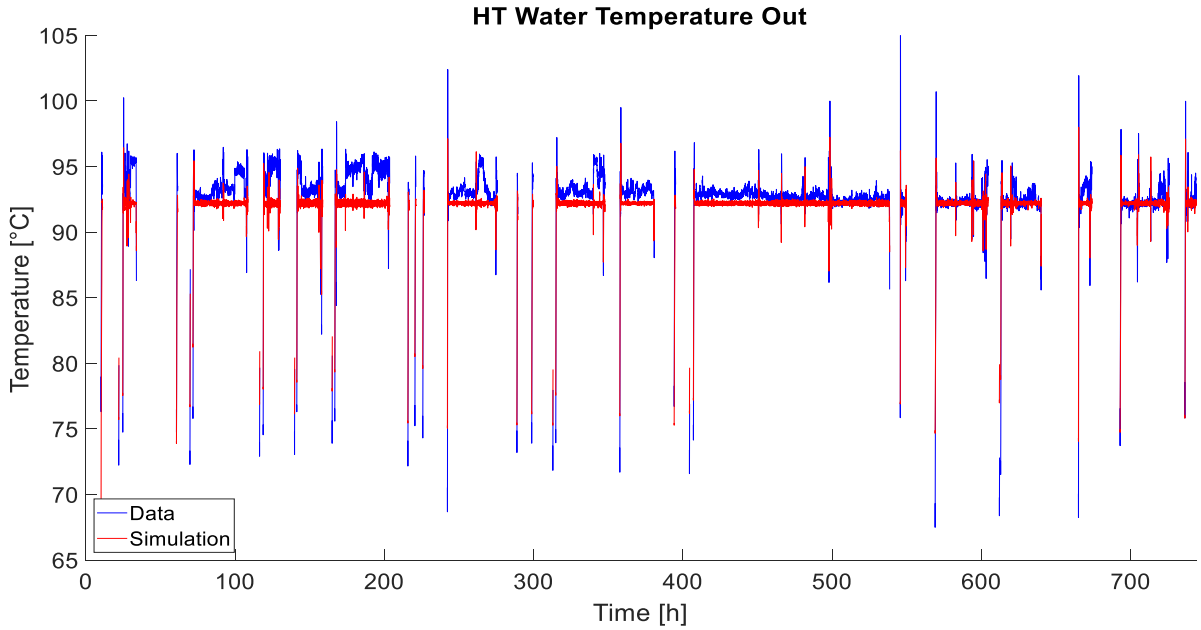

Figure 25 HT temperature after the charge air cooler (data when the engine is offline has been excluded)

8.2.4 Updating heat exchangers and tuning them

First, the lube oil cooler and both charge air coolers were updated and then tuned using 100% load to match the heat balance in the engine product guide. Then the seawater cooler was tuned so that the LT temperature at its outlet matched data. As seen in Figure 26, this proved to be a problem, since no matter what heat transfer coefficient was chosen only some intervals of the simulation matched data, although it still follows the pattern of the data. It seemed to be a combination of high LT water temperature at the inlet and high seawater temperature, but no clear cut off points could be found. The temperature data used for the secondary side of the WHR heat exchanger could be the problem. Due to the sensor closest to the WHR heat exchangers in the WHR-system being faulty, a sensor further away was used instead. While most of the flow passes through that sensor, the temperature could still be quite different closer to the WHR heat exchangers due to other flows in the WHR system.

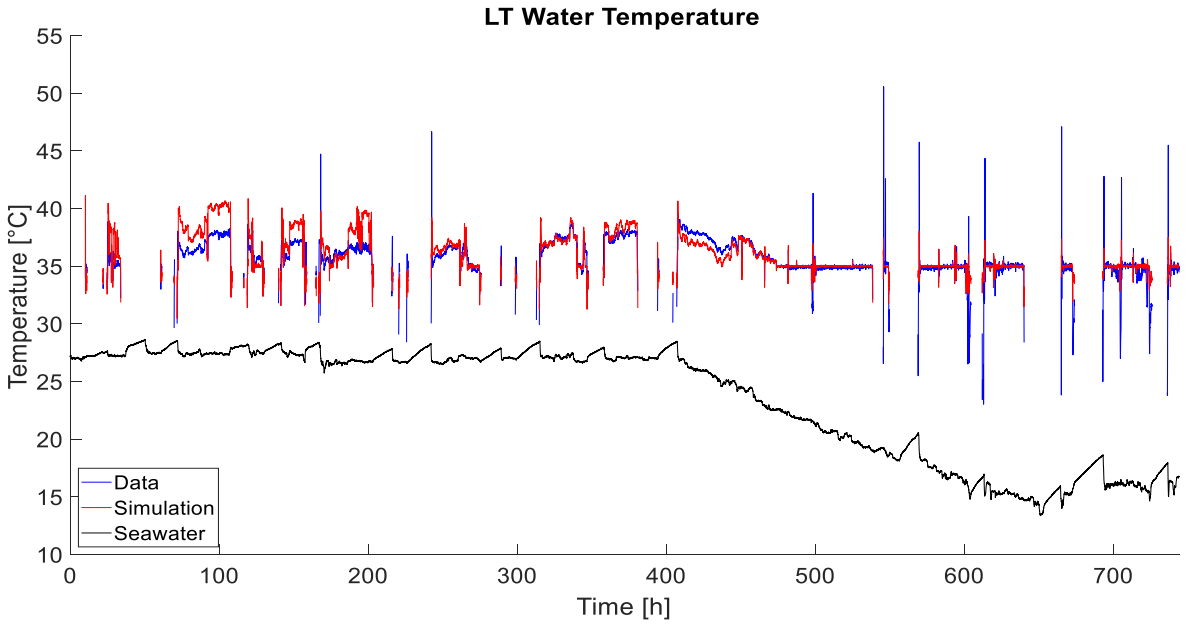

Figure 26 LT water and seawater temperature (data when the engine is offline has been excluded)

8.2.5 Updating setpoints

It was then time to determine the different setpoints. The first temperature control valve setpoint to be tuned was the temperature at the engine outlet. After a few simulation runs with different setpoints, it became clear that there were two different setpoints depending on engine load. Both setpoints were also 1 °C lower when the seawater temperature dropped under a certain level. Figure 27 shows that the simulation follows the data quite well, although there are some deviations, especially in the time interval 260-275 h where the data seems to follow no certain setpoint at all. This interval along with some others seemed to follow the engine load instead of a certain setpoint. There are at least four possible reasons for that. One is that the setpoint is actually dynamic and uses, for example, an interpolated lookup table depending on load. Another reason might be that the sensor that controls the engine temperature is actually located between the jacket and the charge air cooler instead of after the latter. The third is a combination of the first and second. The fourth possible reason that was found later suggests that more heat is transferred from the charge air cooler and that there is an additional setpoint. The last version seemed to be the simplest and most logical reason and was introduced later in the process and is used in the final version of the model.

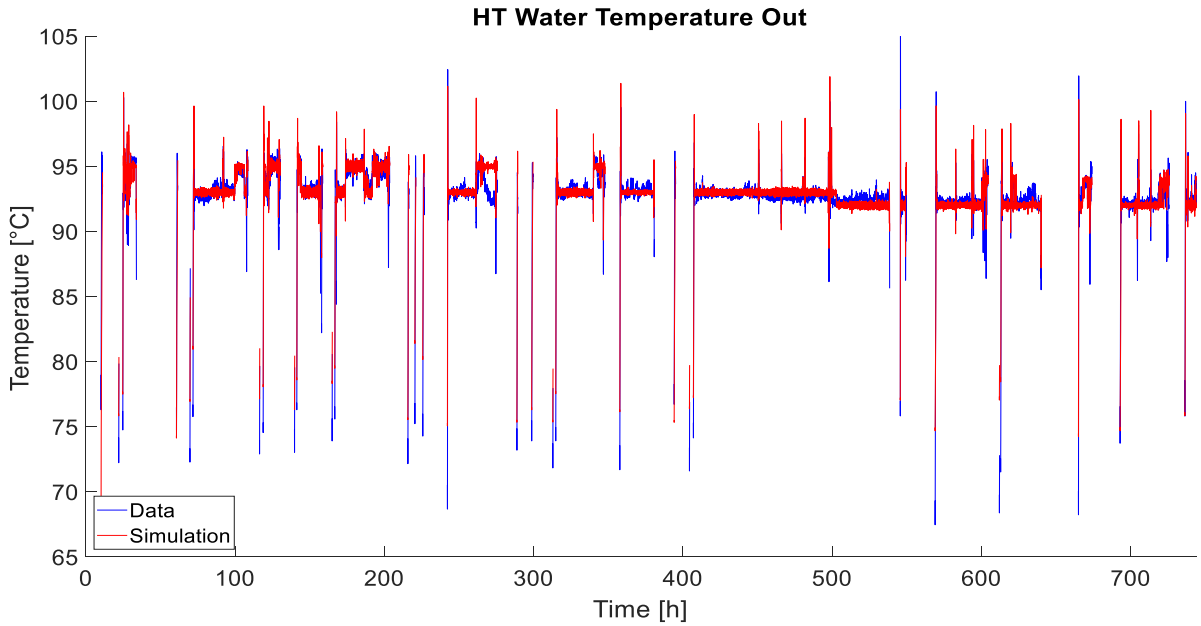

Figure 27 HT temperature after the charge air cooler (data when the engine is offline has been excluded)

The next valve to receive updated setpoints was the temperature control valve for heat recovery. Looking at the data and doing some test runs it seemed like there were two different setpoints, one at high loads and another at lower loads. Figure 28 shows how the simulation compares to the data. The simulation does well for the most part, although there are some parts where the temperature is between the setpoints. Comparing the load with the temperature suggests that the sensor uses an interpolated lookup table. This is discussed later in the chapter.

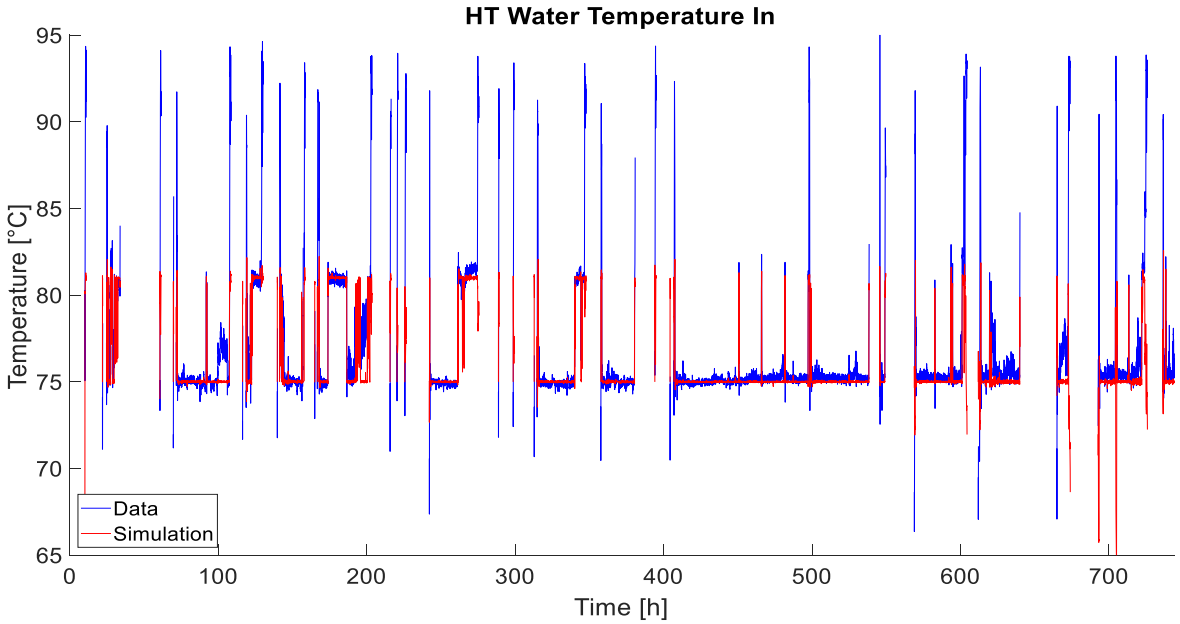

Figure 28 HT temperature after the HT/LT mixing valve (data when the engine is offline has been excluded)

The temperature control valve for the central cooler was the last valve to be tuned. At first, it looked like the larger engines only had one setpoint, but upon closer examination they had short periods of

low loads where the setpoint was different. This did not change much due to the short periods of low load so the simulation still looks like in Figure 26.

To make the model more accurate, an equation for the wall temperature was added to the heat exchanger models. As a result, all heat transfer coefficients had to be tuned again to fit the measurements. Tuning the first stage of the charge air cooler led to the realisation that it had a significant effect on the HT temperature out of the engine. It was quickly noticed that by increasing the heat transfer coefficient the HT water temperature started to follow the measurements more closely. One of the setpoints was changed and the point where the seawater temperature affected the setpoint was also changed. The simulation now managed to partly simulate the strange interval at 260-275 h in Figure 27, which led to the discovery of a possible third setpoint. A small change to the lookup table for the compression ratio of the turbo compressor was made to better simulate that interval. This also made the lookup table more realistic, but it is still a rough estimation and lacks dynamic efficiency since the real table was not accessible.

The setpoints for the temperature control valve for heat recovery were now replaced with the lookup table mentioned earlier. This relatively simple lookup table improved the accuracy of the intervals where the real temperature was not stable.

Since air and liquid water have very different abilities to transfer heat, both flows of the charge air coolers were changed to have different heat transfer coefficients. This required some tuning to adapt the simulation to the measurements.

The following three figures compare the final version of the simulation with data from the reference ship. Figure 29 shows the HT water temperature after the engine. The simulation seems to follow the data well, but is smoother and the largest peaks are lower.

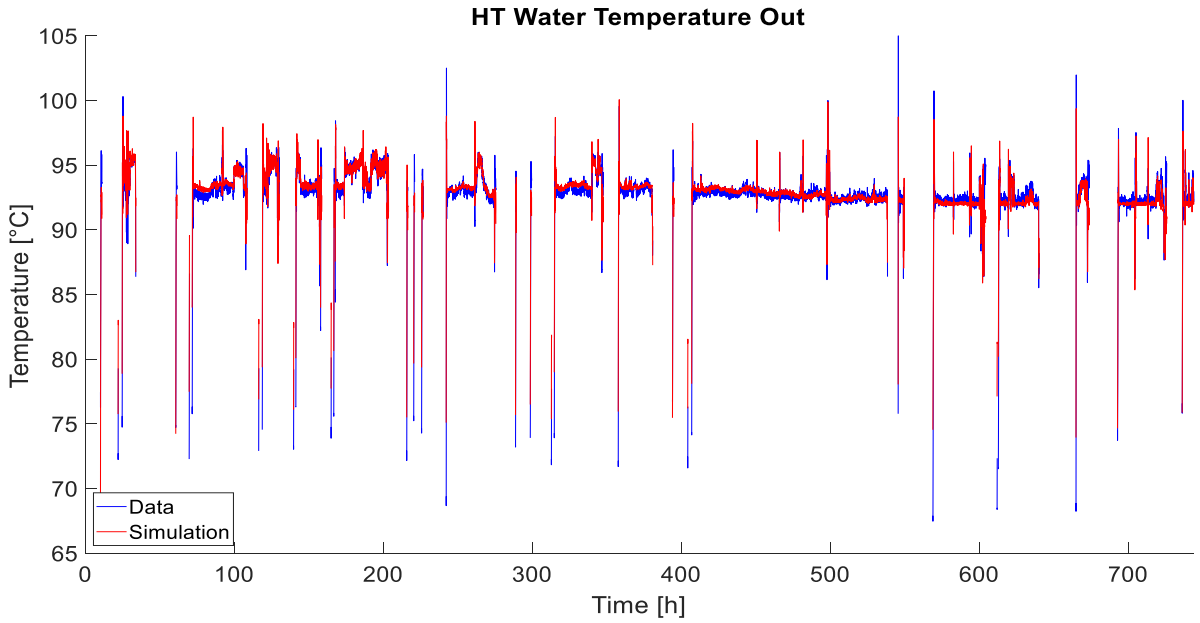

Figure 29 HT temperature after the charge air cooler (data when the engine is offline has been excluded)

Figure 30 presents the temperature of the HT water after the HT/LT mixing valve. The simulation follows the real data very well, but is smoother and has smaller peaks. The smoothness is likely due to the mixing of the HT and LT water being assumed to be perfect and therefore better than the real system.

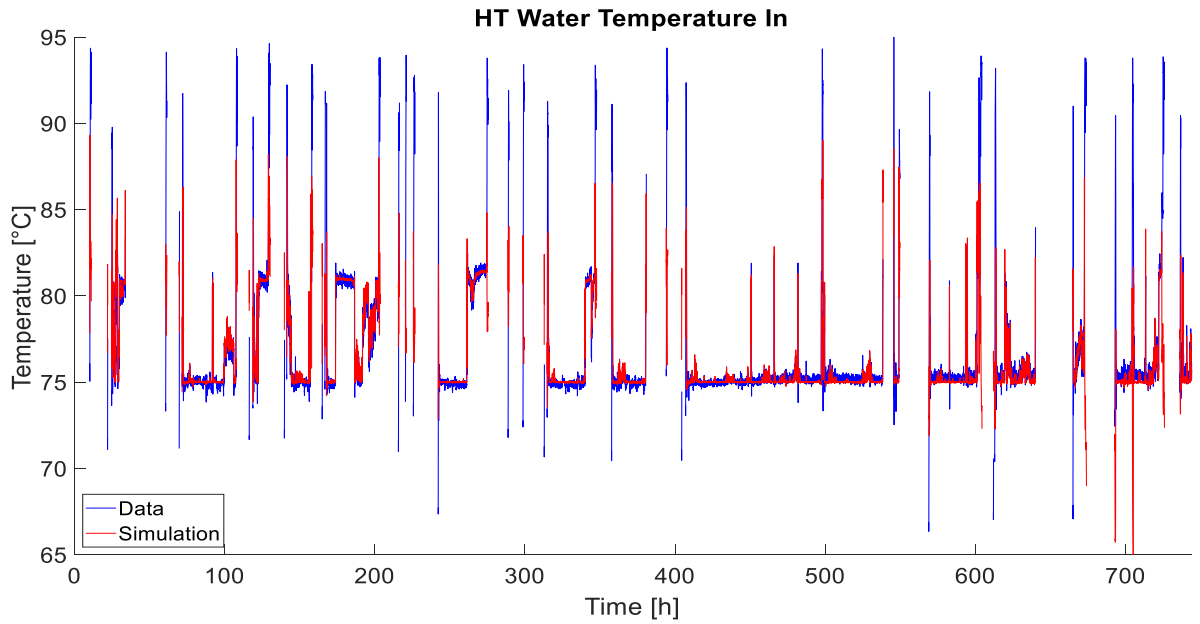

Figure 30 HT temperature after the HT/LT mixing valve (data when the engine is offline has been excluded)

Figure 31 shows the LT water temperature after the seawater cooler. The simulation follows the temperature changes well, but the deviation from the measured value is quite high at some intervals. The possible causes are discussed in the next section.

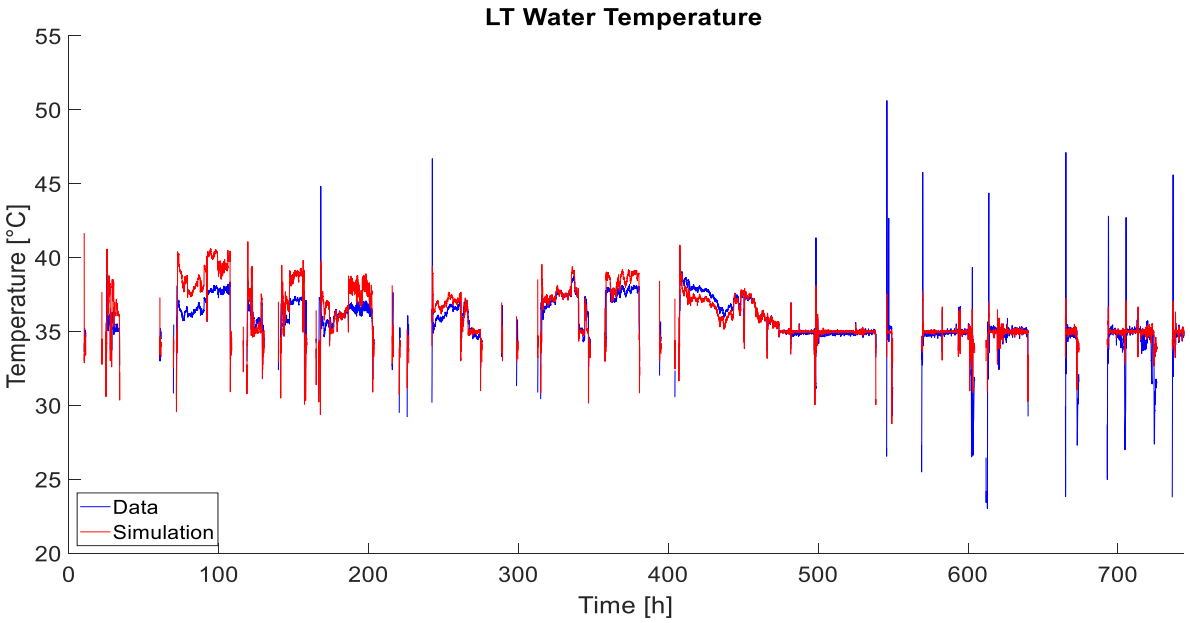

Figure 31 LT temperature after the seawater cooler (data when the engine is offline has been excluded)

8.3 Problems with the LT circuit simulation

While the simulation of the HT circuit works very well, there are some problems with the LT circuit that are still unsolved. It appears to be a complex problem that might have multiple factors contributing to it.

The main problem, which can be seen in Figure 31, is that the temperature deviation varies considerably during the first 450 hours of the trip. During some intervals, the simulation is not able to cool down the LT water enough, while in other intervals it cools it down too much. There are also intervals during those 450 hours where it manages to match the data quite well. This means that changing the heat transfer coefficient will not help, since it would just make the deviations change place. Another problem is that the seawater pump data shows that the seawater flow rate is almost constant during all those time intervals, which means the heat transfer coefficient cannot be made dynamic depending on flow rate. The seawater temperature is also constant during the time period, so the cooling ability should not change much. This means that there is too much heat in the LT water before the seawater cooler.

The question is where the extra heat is coming from. The LT circuit has two direct heat sources and three indirect sources. The direct sources are the second stage of the charge air cooler and the lube

oil cooler while the indirect sources are the engine jacket, the first stage of the charge air cooler and the WHR heat exchanger.

The heat transferred from the lube oil cooler, the second stage of the charge air cooler, and the engine jacket is relatively close to the values reported by the engine guide. The first stage of the charge air cooler shows larger changes, but it seems to have only a minimal effect on the LT water temperature via the charge air. The temperature of the HT water flow to the WHR heat exchanger is relatively stable, as seen in Figure 30, and it does not correlate with the LT water temperature.

The measured temperature of the WHR flow, however, does follow the measured temperature of the LT water flow after the seawater cooler quite well. Even though this temperature is from a sensor further back, it appears to have a notable effect on the seawater temperature. Thus, if the real temperature closer to the WHR heat exchanger is lower, it could perhaps explain the deviations in the LT water temperature. However, simulations showed that the real WHR temperature would have to be several degrees lower to be able to reach the measured LT temperatures. The heat exchangers in the WHR system that do not affect the temperature of the sensor used in the simulation are not capable of cooling the WHR flow enough to reach the temperature needed to reach the measured LT temperature.

While it was possible to obtain a marginally better result using various methods to make the heat transfer coefficient dynamic, it was decided to keep the coefficient static to keep it similar to the other heat exchangers.

9 Validation

Validation is necessary to confirm the accuracy of the model. This is usually done by validating the model against data that was not used when adapting the model, but that was not possible to do for this thesis. Since the seawater temperature changed so much during the trip, the choice was made to use the whole time period for the adaption. However, the fine-tuning of the intervals where the temperature is not stable was done at a single interval. This means that the data used for the adaption can still be used for the validation. Since the reference ship has two pairs of engines, the other engine of the same size (DG3) is also used to validate the model using the same parameters.

While Simulink ran the simulation using flexible step sizes, it was configured to only output every 60 seconds to match the actual measurements. This gave 44 640 data points per signal to work with.

9.1 Validation results

The outputs from Simulink and the outputs from the real system were imported into MATLAB so they could be analysed.

First, the data used for adaption is validated. Since the model does not properly simulate the system during the times the engine was off, two sets of data will be used: the full dataset and a dataset that ignores the data points when the engine was turned off.

Figure 32 shows the temperature error of both datasets. Most of the large errors occur when the engine is offline, which is expected due to the delimitation chosen in the thesis. The large errors that occur during operation usually happen during startup or shutdown. The exception is the LT water that has been discussed earlier.

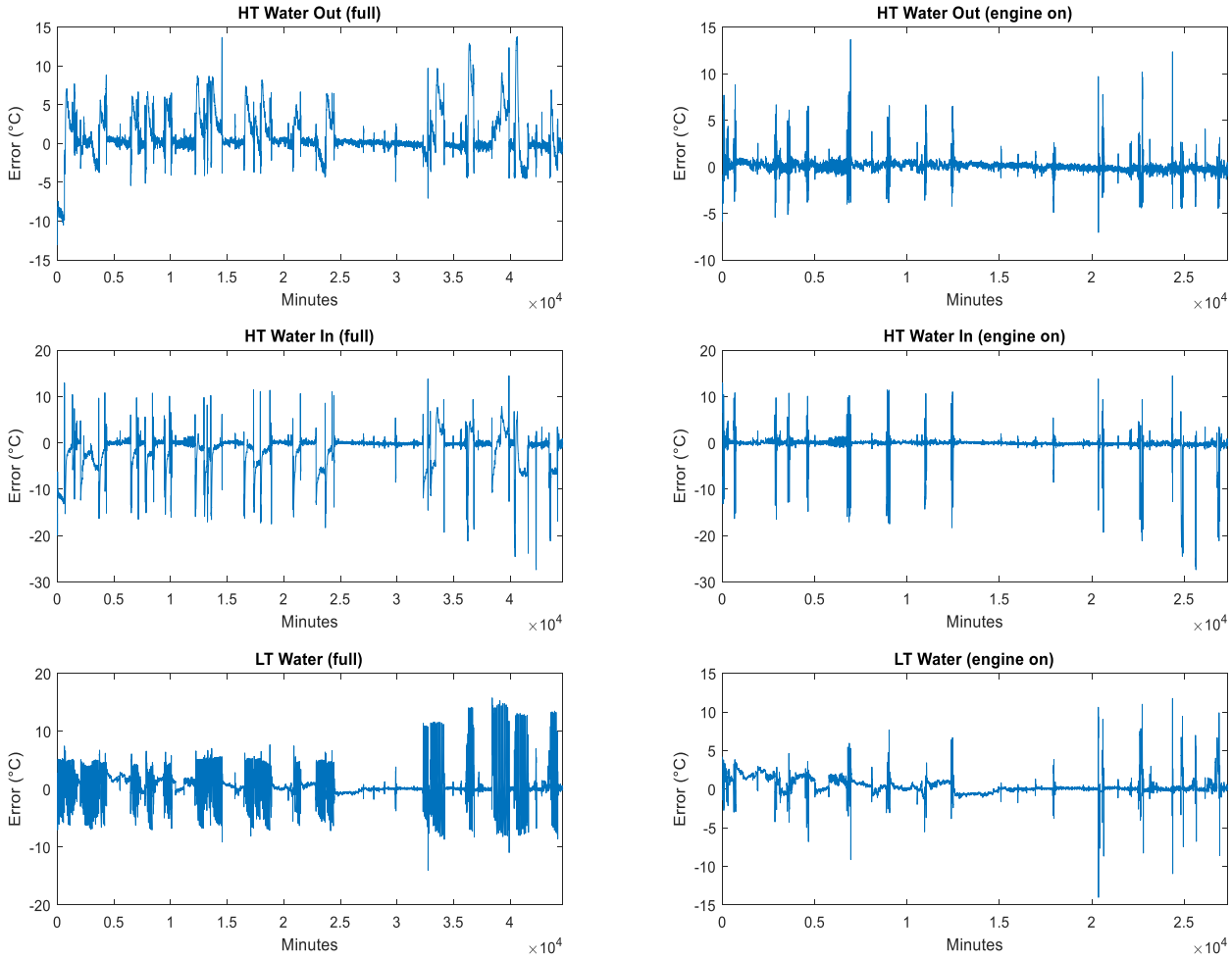

Figure 32 Error of simulation data compared to validation data

In Table 5, the mean and mean absolute errors are presented. The mean absolute errors when the engine is online are very good. Even though the simulation of the LT water flow has problems during quite a large part of the journey, it has a lower mean absolute error than the HT water before the engine. This suggests that the HT water before the engine has much larger peaks than the LT water.

Table 5 Mean and mean absolute errors

	Mean error (°C)	Mean absolute error (°C)
HT Water Out (full)	0.87	1.68
HT Water Out (engine on)	0.07	0.45
HT Water In (full)	-1.68	2.22
HT Water In (engine on)	-0.55	0.87
LT Water (full)	0.37	1.79
LT Water (engine on)	0.39	0.70

Figure 33, Figure 34 and Figure 35 show histograms of the error distributions. They have been truncated to more clearly show the mean value. The complete histograms are shown in Appendix A.

Figure 33 shows the error distribution of the HT water temperature after the charge air cooler. While there are quite many errors larger than 2 °C, these occur when the engine is offline. The vast majority of the errors during operation are very small.

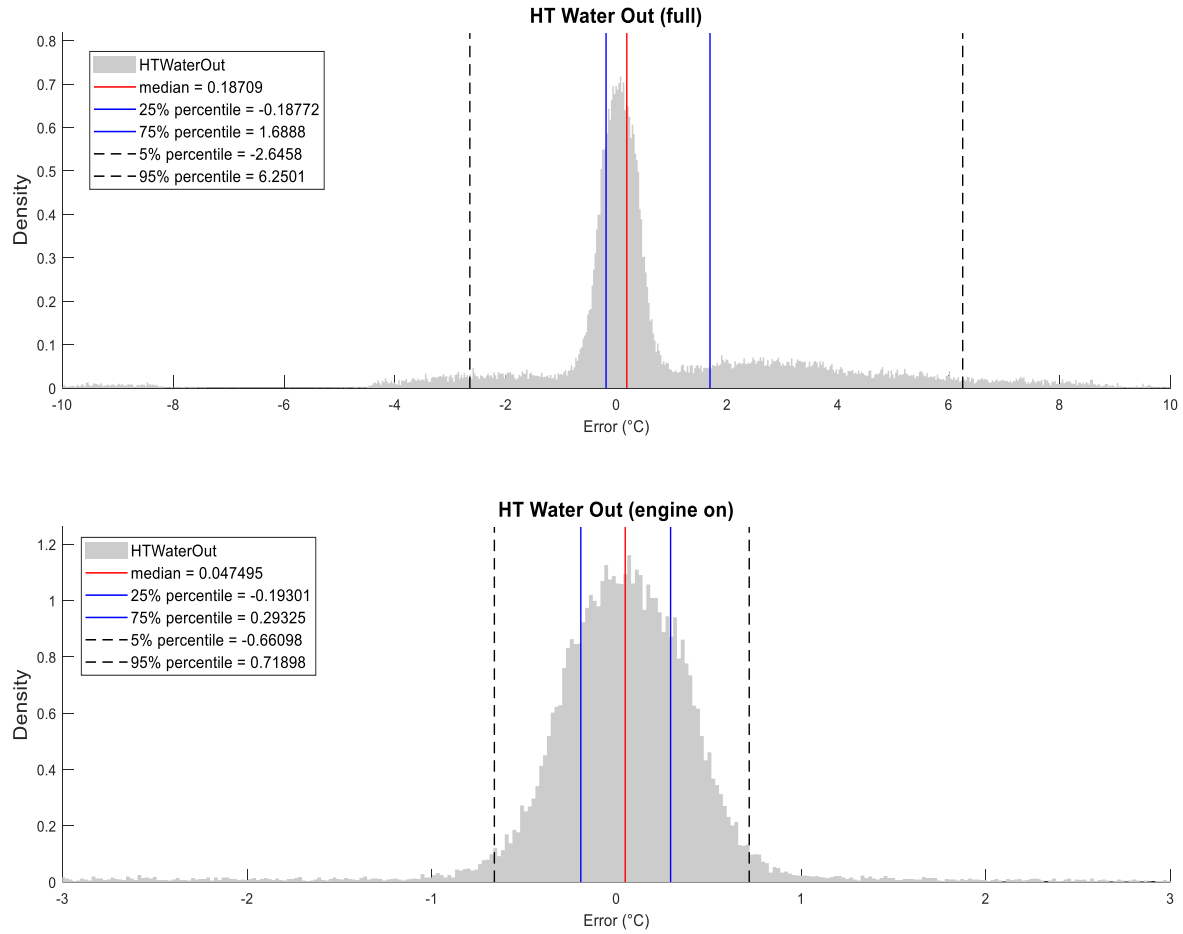

Figure 33 Histograms of the error for HT water temperature after the charge air cooler (truncated)

The error distribution of the HT water temperature after the HT/LT mixing valve is shown in Figure 34. The majority of the large errors occur when the engine is not running. The errors during operation are very small.

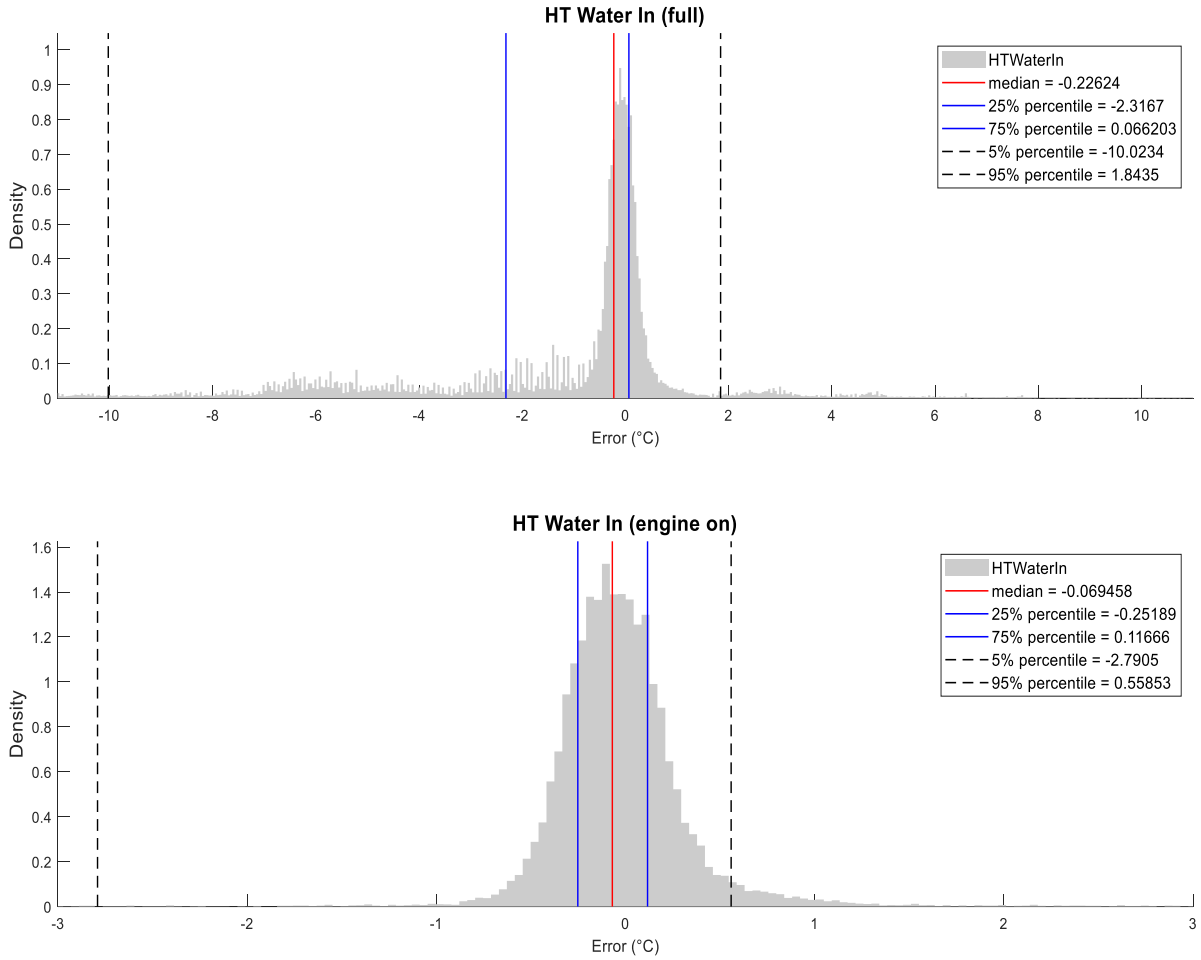

Figure 34 Histograms of the error for HT water temperature after the HT/LT mixing valve (truncated)

Figure 35 shows the error distribution of the LT water temperature. The full data set has quite many large errors, both positive and negative, due to the wildly changing measured temperature when the engine is turned off. During operation the simulation works better, but there are still relatively many errors, mostly on the positive side due to the problems mentioned in Section 8.3.

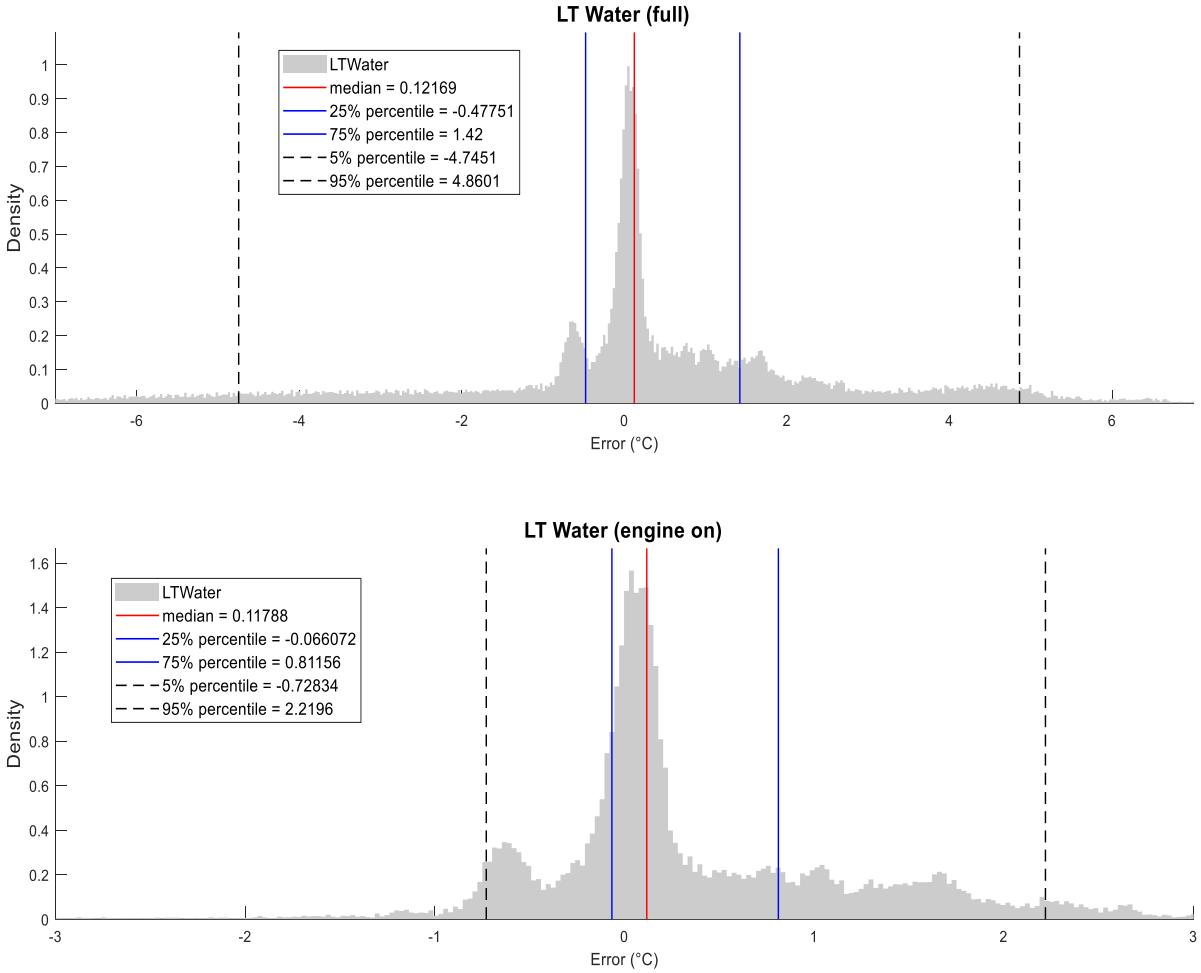

Figure 35 Histograms of the error of the LT water temperature (truncated)

The data from the other engine of the same size, DG3, was also used to validate the model. Everything in the model was kept the same, except the engine specific inputs. These were engine power and charge air temperature.

The following three figures compare the simulation with the data from DG3. The HT water temperature after the engine is shown in Figure 36. The simulation seems to follow the data well when the engine is running, although the simulation temperatures are slightly too high.

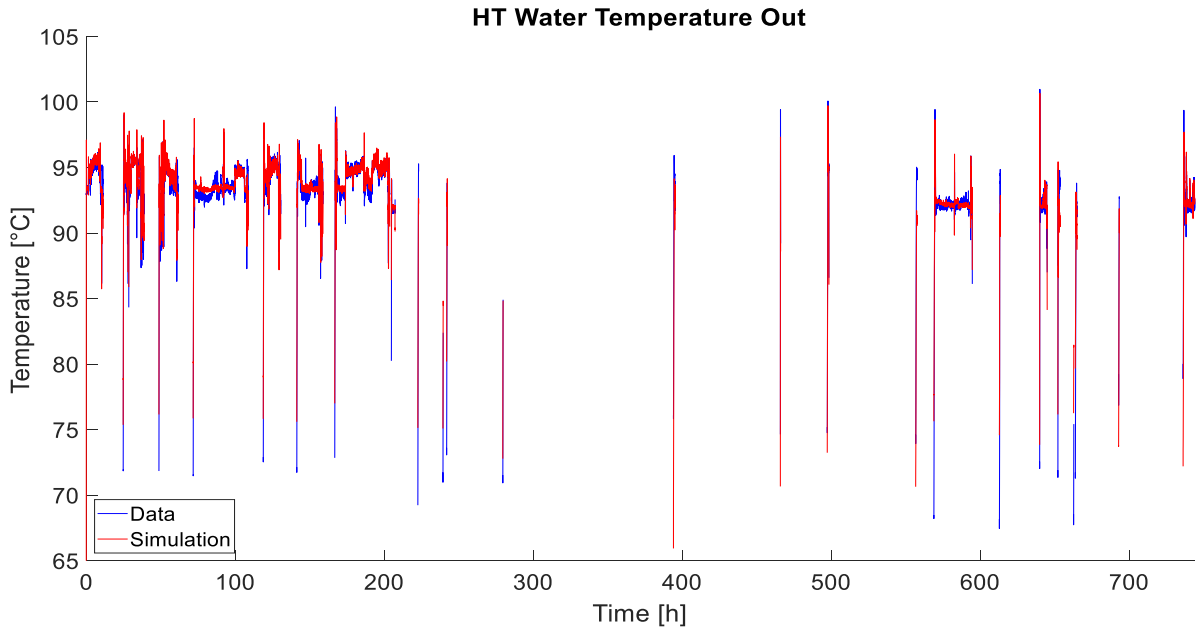

Figure 36 HT temperature after the charge air cooler (data when the engine is offline has been excluded)

Figure 37 shows the HT water temperature after the HT/LT mixing valve. This also follows the data well, but like the HT temperature after the charge air cooler, the simulation temperatures are slightly too high during periods when the measured temperatures are not stable. Since the model was adapted to DG1, this likely means that the setpoints are slightly different. This is what causes the difference in the HT temperature after the charge air cooler. The simulation is smoother with smaller spikes.

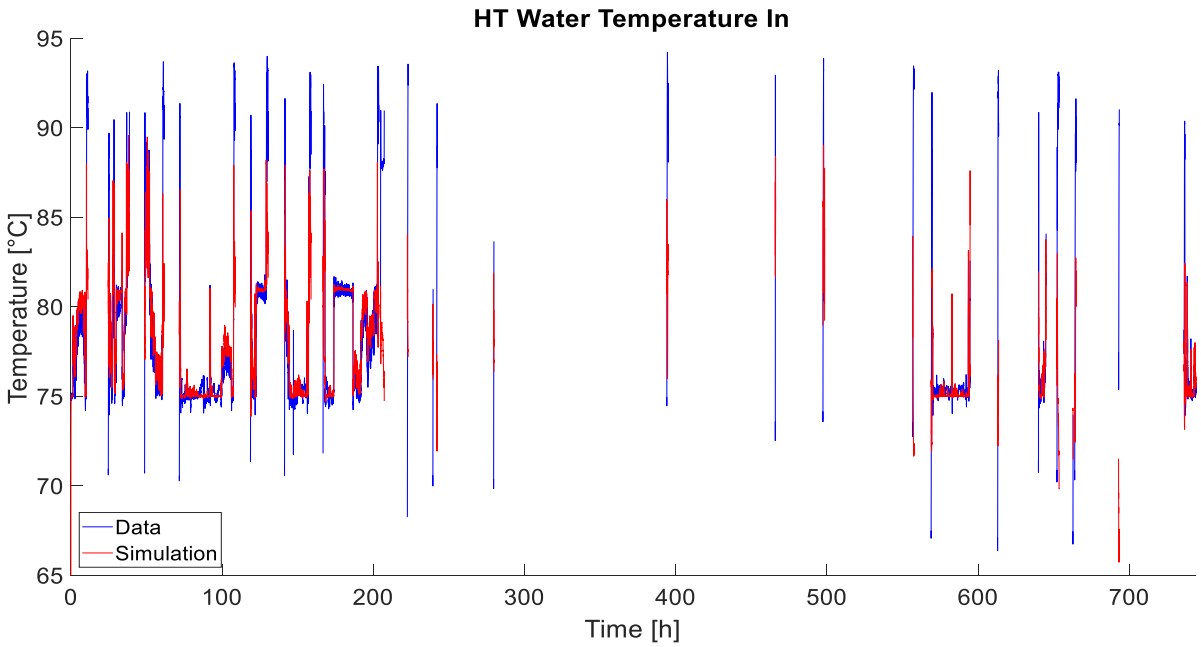

Figure 37 HT temperature after the HT/LT mixing valve (data when the engine is offline has been excluded)

The LT water temperature after the seawater cooler is shown in Figure 38. Like DG1, the simulation follows the temperature changes quite well, but the temperature difference is rather high.

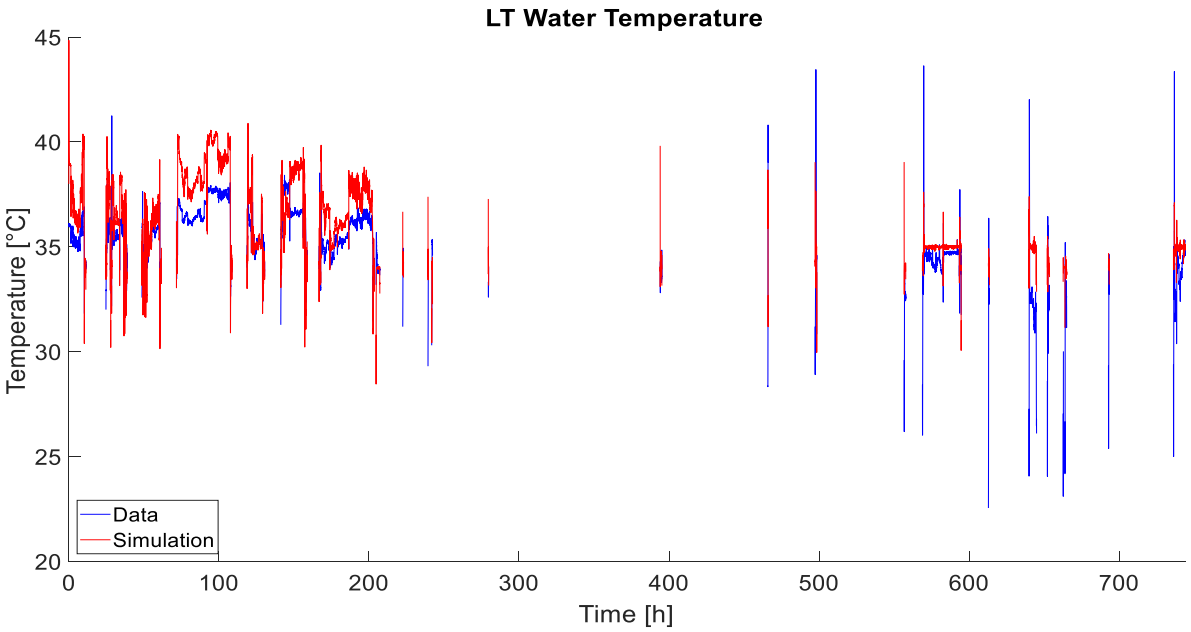

Figure 38 LT water temperature after the seawater cooler (data when the engine is offline has been excluded)

Figure 39 shows the errors of DG3. The very large error in the beginning of the "HT Water Out" graphs due to the starting value is not shown to emphasize the rest of the errors. As with DG1, most of the errors occur when the engine is offline due to the delimitation set for the thesis. During operation, the errors are generally very small for both HT temperatures. The large errors occur during start up and shutdown, although the HT water temperature after the HT/LT mixing valve has some intervals were the simulation temperature is several degrees lower than the measured temperature for a couple of hours. These occur when the engine is running at a very low load. Some test simulations with higher setpoints for low loads were run to try and solve the problem, but it was impossible. This might indicate that the HT flow is lower when the engine is running at very low loads.

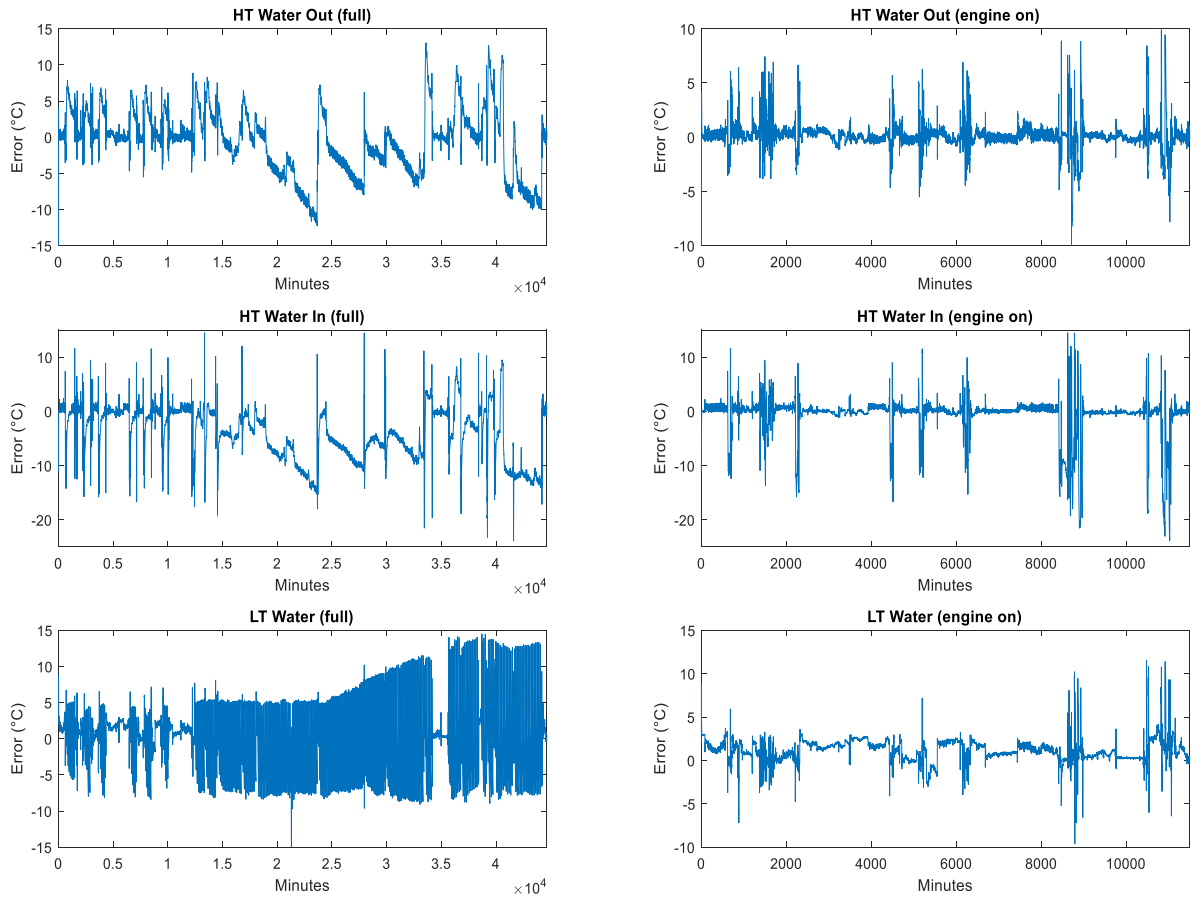

Figure 39 Error of simulation data compared to validation data

Table 6 shows the mean and mean absolute errors of the simulation of DG3. The mean absolute errors of the full set of this engine are much larger than those of DG1, which is expected due to it being used much less so the properly simulated time period is shorter and not being the one the parameters were adapted for. This also applies to the errors when the engine is running. The shorter operation period also make the large errors affect the mean much more.

Table 6 Mean and mean absolute errors

	Mean error (°C)	Mean absolute error (°C)
HT Water Out (full)	-0.68	3.33
HT Water Out (engine on)	0.17	0.71
HT Water In (full)	-4.14	4.75
HT Water In (engine on)	-0.78	1.62
LT Water (full)	-0.39	3.32
LT Water (engine on)	1.13	1.37

Figure 40, Figure 41 and Figure 42 show histograms of the error distributions. They have been truncated to more clearly show the middle part. The complete histograms are shown in Appendix B.

Figure 40 shows the error distribution of the HT water temperature after the charge air cooler. The simulation of the full data set is quite a lot worse than for DG1, but this is mostly due to the engine not being in use much. The errors during operation small, although they are a little larger than for DG1. These seem to be caused by the slightly different setpoint lookup table of the HT water temperature after the HT/LT mixing valve.

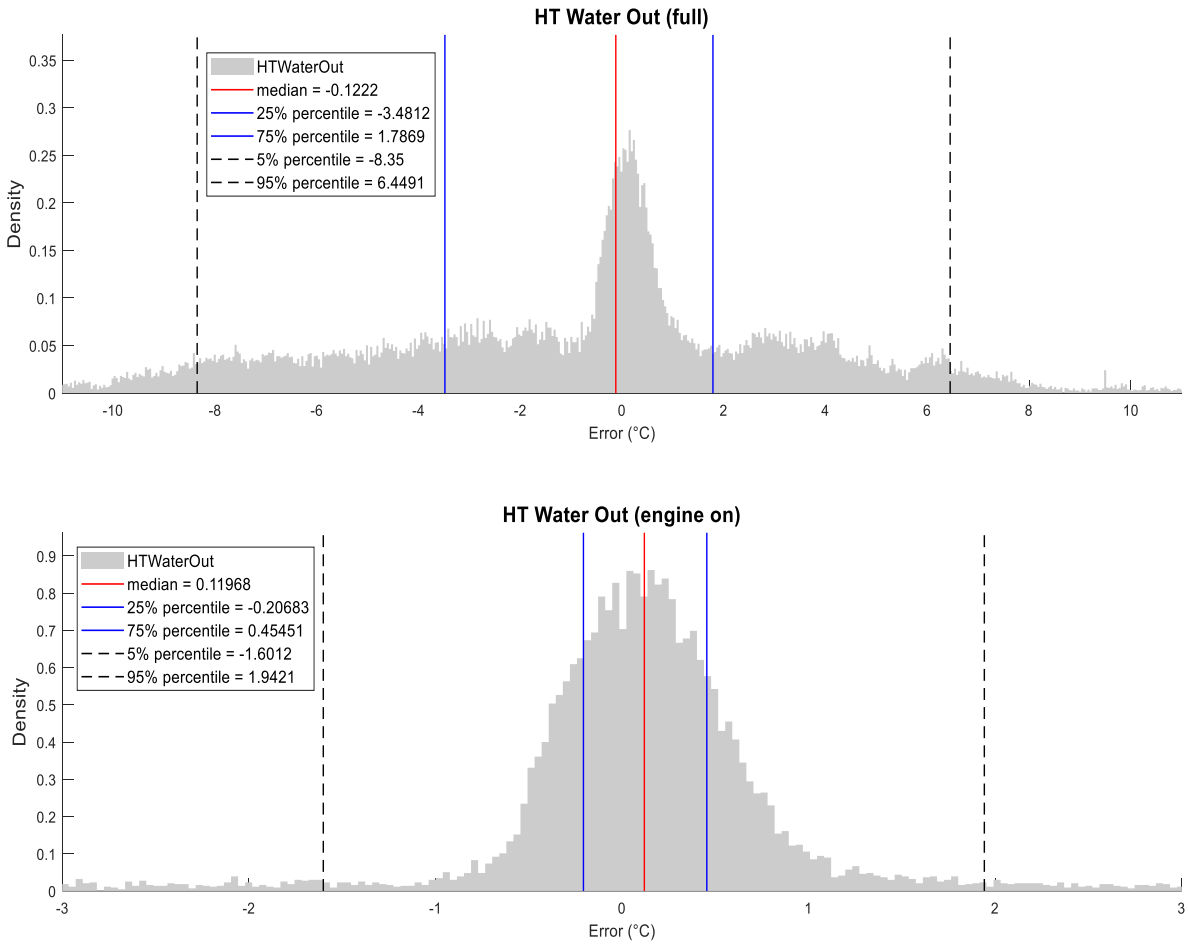

Figure 40 Histograms of the error for HT water temperature after the charge air cooler (truncated)

The error distribution of the HT water temperature after the HT/LT mixing valve is shown in Figure 41. There are numerous large errors in the full data set due to the engine being offline most of the time. The simulation during times when the engine is online is very good, though. The relatively large number of errors between 0.52 and 1.37 occur during times when the setpoint is not stable at a certain temperature. Since the model was adapted for DG1, the setpoint lookup table for this engine might be slightly different and therefore causing the errors. The quite large number of large negative errors occurs when the engine is started/stopped and when it is run on low loads.

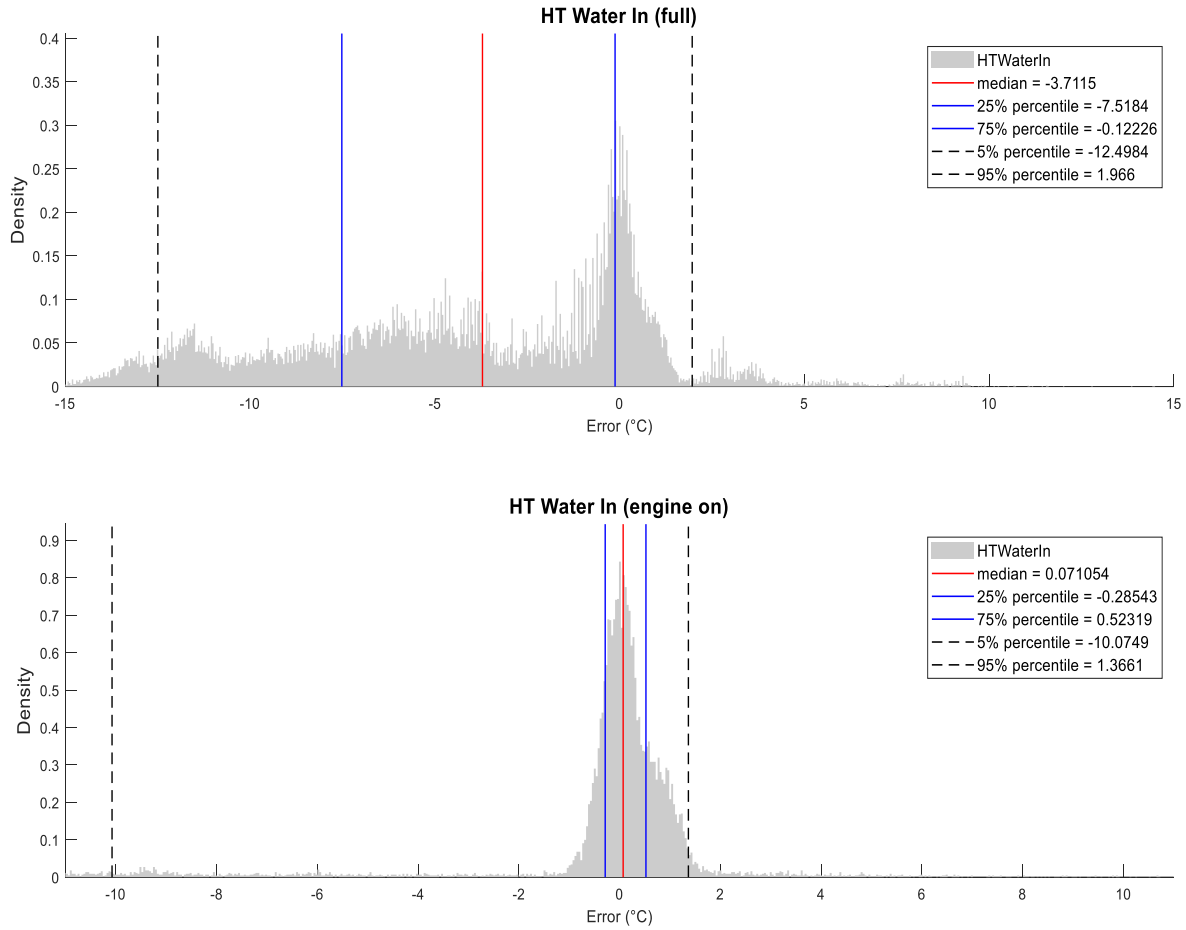

Figure 41 Histograms of the error for HT water temperature after the HT/LT mixing valve (truncated)

Figure 42 shows the error distribution of the LT water temperature. The full data set has numerous large errors, both positive and negative, due to the wildly changing measured temperature when the engine is turned off. During operation the simulation works better, but there are still relatively many errors, mostly on the positive side due to the problems mentioned in Section 8.3. These are quite similar to those of DG1, but accentuated due to the much shorter operation period.

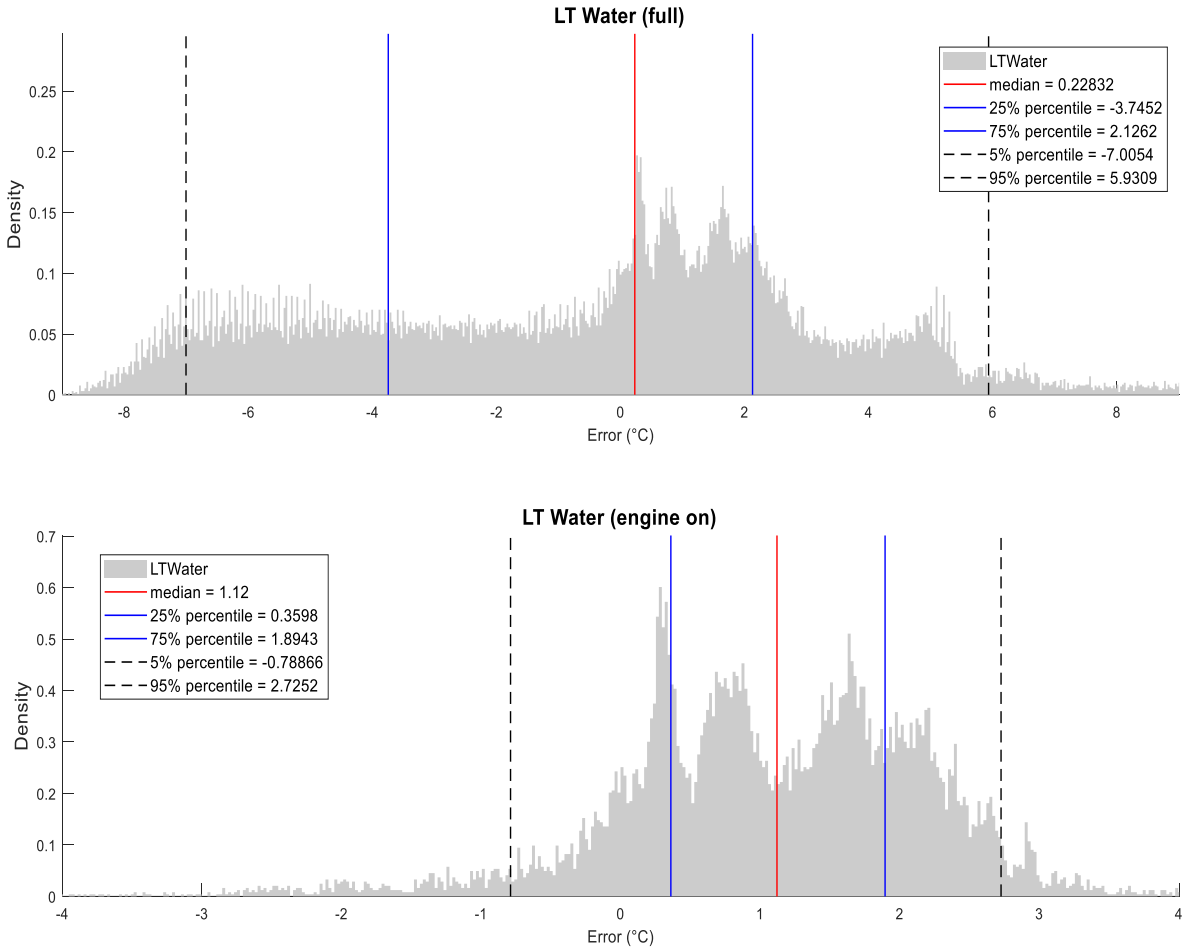

Figure 42 Histograms of the error of the LT water temperature (truncated)

The simulations were done using variable time steps. This usually resulted in about 125 000 iterations for DG1 and about 105 000 for DG3. Running the simulations on a quad-core Intel i5-4570 takes about four to five minutes, which is around 10 000 times faster than real time. This is, however, a simple model of just one engine in isolation. Adding all four engines to a simplified version of the WHR system resulted in a simulation speed of about 90 minutes, which is still about 500 times faster than real time. A simulation of the four engines together took about 47 minutes.

9.2 Conclusion of validation

Naturally, the simulation results will never be completely accurate due to simplifications made to the model. The mean absolute errors in Table 5 and Table 6 and the “engine on” histograms of Figure 33-Figure 35 and Figure 40-Figure 42 confirm that the model is still quite accurate. Especially the HT temperature simulations are accurate during engine operation.

The main reasons for the deviations are simplifications. For example, the preheating during standby is not simulated and the flows are either constant or based on very rough approximations. This especially affects the LT temperature.

10 Conclusion

In this thesis, the goal was to provide insight into what data is needed to run dynamic simulations of a ship engine cooling system model and to adapt and validate said model.

Only five input sensors for the engine cooling system were found in the data, which was a small problem. This meant that although the data was enough for quite accurate dynamic simulations, it was not possible to test whether more data would have improved the accuracy or not.

The validation results of both HT temperatures are promising. They show that it is possible to simulate the HT circuit well even with a relatively simple model and few inputs. It also proved to be possible to run simulations of DG3 by just changing the engine specific input data, but keep all other parameters the same as for DG1. The simulation results of DG3 were slightly less accurate, likely due to the shorter operation time accentuating the errors during start up and shutdown rather than the model being less accurate.

The simulation of the LT circuit is, however, not as accurate. While the simulated temperature does follow the pattern of the measured data, there are relatively large deviations. Similar deviations happen during the simulation of DG3. Various explanations to the issue are presented in Section 8.3, but the problem appears to be complex and no solution was found.

With more data, it would be possible to expand this model. For example, by adding the WHR system to the model it would be possible to properly simulate the engine cooling system during the time periods when the engine is offline. Another example would be to simulate all four engines connected to the WHR system. While it was already possible to simulate all engines connected to a simplified version of the WHR system, an issue with the sensor measuring the WHR water temperature after the cooling systems meant that it was not possible to validate it.

Summary in Swedish – Svensk sammanfattning

Validering av en digital tvilling för ett fartygsmotorkylsystem

Energieffektivitet blir hela tiden viktigare och viktigare för rederier, skeppsbyggare och forskare, både på grund av striktare internationella marina krav och ökande bränslekostnader. Alla fartyg över 400 GT byggda efter 1 januari 2013 måste följa ett energieffektivitetsindex (EEDI) genomdrivet av den internationella sjöfartsorganisationen IMO (International Maritime Organization) för att sänka koldioxidutsläppen genom att minska på bränsleförbrukningen. EEDI kommer att bli striktare vart femte år med början 2015, vilket kräver kontinuerlig utveckling av fartygen för att möta kraven. Detta gör nya fartyg dyrare att bygga, men man förväntar sig att bränslebesparingen kommer att kompensera för de extra investeringskostnaderna (IMO, u.da.; ICCT, 2011).

Den 1 januari 2020 sänktes gränsen för SO_x och luftburna partiklar kraftigt utanför svavelkontrollområden (SECA), från 3,50 massprocent till 0,50 massprocent. Inom SECA har gränsen varit 0,10 massprocent sedan 1 januari 2015 (IMO, u.db.). Det här tvingar rederierna att installera skrubbrar eller byta till bränsle som innehåller mindre svavel. Fartyg med skrubber kan fortsätta använda billigt högsvavligt bränsle, medan resten av fartygen måste byta till dyrare lågsvavligt bränsle för att uppfylla utsläppskraven. De ökade bränslekostnaderna är en av orsakerna till att marinindustrin fokuserar mer och mer på energieffektivitet.

Det finns många metoder som kan användas för att öka effektiviteten, men de flesta fokuserar på endast en del av energisystemet. Målet med detta arbete är att försöka råda bot på detta genom att anpassa och validera en enkel digital tvilling av ett fartygs motorkylningssystem på data från ett fartyg. Eftersom motorerna i standby är starkt beroende av förvärmning via värmeåtervinningssystemet beaktas enbart hur simuleringen fungerar då motorerna är igång.

En digital tvilling är en virtuell kopia av en fysisk process, system eller produkt. Den är konstruerad för att agera som en bro mellan den fysiska och den digitala världen. Den digitala kopian, som byggts upp genom att använda mätningar från ett system, kan användas för att t.ex. analysera eller optimera det fysiska systemet (Monteith, 2019; Shaw & Fruhlinger, 2019).

Arbetet fokuserade på den viktigaste delen i ett kylningssystem, värmeväxlarna. En värmeväxlare är en apparat som används för att överföra värme mellan två eller fler fluider (vätska eller gas) med olika temperaturer. Enligt termodynamikens andra huvudsats flödar energin alltid från den varma fluiden till den kalla fluiden. Några typiska applikationer för värmeväxlare inom energi- och marinindustrin är

uppvärmning eller nedkylning av ett visst flöde, värmeåtervinning eller evaporerering eller kondensering av något flöde.

Fartyget vars data används i avhandlingen har fyra motorer i två par med samma cylinderdiameter, men olika cylinderantal. Alla motorer har varsitt kylsystem, där bl.a. värmeväxlarnas storlek skiljer sig mellan de två större och de två mindre mototerna, men upplägget är det samma. En högtemperaturkrets som kyler cylinderfodret, topplocket och första steget i laddluftkylaren och en lågtemperaturkrets som kyler smörjoljan och det andra steget i laddluftkylaren. En enkel version av kylsystemet visas i Figur 14. Alla fyra kylsystem är kopplade till samma värmeåtervinningssystem via värmeåtervinningsvärmeväxlarna (waste heat recovery HE i Figur 14). Högtemperaturkretsen kyls av värmeåtervinningssystemet och lågtemperaturkretsen kyls i sin tur av havsvattnet.

I kylsystemet finns fem ventiler som styrs av regulatorer med hjälp av temperatursensorer och en som styrs manuellt. Dessa visas i Figur 15 där ventilerna är 1-6, temperatursensorerna T1-5 och regulatorerna P1-5.

Simulink användes som program för att simulera motorkylningsmodellen. Det valdes som simuleringsprogram för avhandlingen eftersom det är ett standardverktyg som används både i industrin och i högskolor.

Det första steget i arbetet var att gå igenom stora mängder sensordata från fartyget för att reda ut vilka sensorer som behövdes för att kunna simulera modellen och vilka som behövdes för att kunna anpassa och validera den. Fem sensorer ansågs vara relevanta för själva simuleringen: motoreffekt, turbokompressorns inloppstemperatur, havsvattentemperaturen, värmeåtervinningsvattnets flödeshastighet och värmeåtervinningsvattnets temperatur. Det fanns dock vissa problem med de två senare. Flödeshastighetssensorn rapporterar hela flödet, så en grov estimering baserat på det totala flödet gjordes. Temperatursensorn i värmeåtervinningsvattnet som ligger närmast värmeväxlarna kopplade till kylsystemen var felaktig, så en sensor längre bak användes istället. Temperatursensorerna som användes för anpassning och validering är T1, T2 och T5 i Figur 15.

En enkel modell av kylsystemet med statiska insignaler gjord av Manngård, et al. (2019) användes som bas för arbetet. Detta gjorde att fokus kunde läggas på att anpassa modellen istället för att bygga den. Eftersom alla motorer hade samma cylinderdiameter kunde arbetet fokusera på en motor. Den som valdes var motor nummer 1 (DG1), eftersom den hade högst användningsgrad.

Anpassningsarbetet började med att uppdatera parametrar i modellen med hjälp av motorns produktguide, bland annat massflödena i både den varma och den kalla kretsen. Nästa steg var att använda data från de ovannämnda sensorerna för att göra de statiska insignalerna dynamiska.

Laddluftflödet gjordes dynamiskt genom att kombinera data från produktguiden med motorbelastningen. Eftersom turbokompressorns kompression och värmeväxlarnas värmekoefficienter var okända ändrades de kontinuerligt för att anpassa simuleringen till mätdata.

Sensorn som mäter varmvattentemperaturen efter motorn antogs först vara belägen mellan själva motorn och laddluftkylaren, men den visade sig vara belägen efter laddluftkylaren. Detta orsakade ett problem, eftersom simuleringstemperaturen var flera grader högre än mätdata. Problemet visade sig vara energifördelningen i modellen, för mycket värme tillfördes båda kylkretsarna. Detta orsakades av att värme från laddluftkylarna överfördes till kylkretsarna två gånger, både från motorn eller smörjoljan och från själva laddluftkylarna. Efter att detta ändrades sjönk simuleringstemperaturen till rätt nivå.

Slutskedet av anpassningen handlade till stor del om att fastställa börvärdena för regulatorerna genom att jämföra simuleringen med data eftersom de verkliga värdena inte var tillgängliga. Eftersom vattentemperaturen före motorn beror mycket på belastningen används en enkel uppslagstabell för att göra börvärdet dynamiskt. Temperaturen efter motorn beror till stor del på laddlufttemperaturen och klarar sig därmed med några få olika börvärden som beror på belastning och havsvattentemperaturen. Temperaturen i lågtemperaturkretsen har två börvärden som beror på belastningen.

Medan simuleringen av högtemperaturkretsen fungerar bra, fanns det vissa problem i lågtemperaturkretsen. Problemet, som kan ses i Figur 31, är att det finns stora temperaturskillnader jämfört med mätdata under de 450 första timmarna. Under vissa intervall klarar simuleringen inte av att kyla ner flödet tillräckligt mycket, medan i andra kyls flödet ner för mycket. Detta betyder att problemet inte går att lösa genom att ändra värmeöverföringskoefficienten, eftersom detta endast leder till att felen flyttar på sig. Både havsvattenflödet och havsvattentemperaturen är så gott som konstanta, vilket betyder att kylförmågan inte borde ändras. Det kommer alltså för mycket värme in i kylsystemet, men ingen lösning på detta hittades.

Validering är nödvändigt för att kunna bekräfta modellens noggrannhet. Data från båda motorerna med samma cylinderantal användes för valideringen av modellen.

Histogrammen för den första motorn ses i Figur 33-35 där ”engine on” är mest relevant, eftersom arbetet fokuserade på tiden då motorerna körs. Simuleringen av båda temperaturerna i högtemperaturkretsen är väldigt nära mätdata, medan temperaturen i lågtemperaturkretsen har relativt stora fel på grund av det tidigare nämnda problemet.

Den andra motorn (DG3) simulerades genom att ändra motorspecifika input, medan resten hölls samma som för DG1. Histogrammen visas i Figur 40-42. DG3 har lite större fel än DG1 i båda kylkretsarna, men felen är fortsatt små i högtemperaturkretsen. Skillnaden orsakas främst av att motorn används under ett färre antal timmar än DG1, vilket gör att felen vid t.ex. start och stopp, förstärks, men det kan även vara att DG3 har små skillnader i t.ex. börvärden.

Valideringsresultaten för högtemperaturkretsen är lovande, de visar att det är möjligt att simulera högtemperaturkretsen med en relativt enkel modell. Simuleringen av lågtemperaturkretsen var inte lika bra, men det kan eventuellt lösas med mera data.

Med tillgång till mera data kunde modellen utökas, t.ex. genom att lägga till värmeåtervinningssystemet och därmed kunna simulera kylsystemet även då motorn är avstängd eller simulera alla fyra motorer samtidigt. Det senare var möjligt redan i denna avhandling, men eftersom temperatursensorn efter värmeåtervinningsvärmeväxlarna inte fungerade, var det inte möjligt att anpassa eller validera.

References

Barlas, Y., 1996. Formal aspects of model validity and validation in system dynamics. *System Dynamics Review,* 12(3), pp. 183-210.

Çengel, Y. A. & Ghajar, A. J., 2015. *Heat and Mass Transfer: Fundamentals and Applications.* 5 ed. New York, New York: McGraw-Hill Education.

da Silva, F. J., 2015. *Dynamic Process Simulation: When do we really need it?.* [Online]
Available at: http://processecology.com/articles/dynamic-process-simulation-when-do-we-really-need-it
[Accessed 16 August 2019].

Engine manufacturer, 2019. *Engine product guide.* s.l.:s.n.

Fortum Heat and Power, 2019. *Apros Thermal.* [Online]
Available at: https://www.fortum.com/sites/g/files/rkxjap146/files/documents/apros-thermal-datasheet.pdf
[Accessed 23 August 2019].

FreeDyn, 2019. *FreeDyn.* [Online]
Available at: http://www.freedyn.at/
[Accessed 23 August 2019].

Glos, J. W., 1997. *Digital Augmentation of Keepsake Objects: A Place for Interaction of Memory, Story, and Self.* Cambridge, MA: Massachusetts Institute of Technology.

Google Scholar, 2019. *Google Scholar search for "digital twin" in title.* [Online]
Available at: https://scholar.google.com/
[Accessed 27 September 2019].

Google Trends, 2019. *Google Trends search for "digital twin".* [Online]
Available at: https://trends.google.com/trends/explore?date=all&q=%22digital%20twin%22
[Accessed 27 September 2019].

Grieves, M., 2011. *Virtually perfect: Driving innovative and lean products through product.* Cocoa Beach, FL: Space Coast Press.

Grieves, M. & Vickers, J., 2017. Digital Twin: Mitigating Unpredictable, Undesirable Emergent Behavior in Complex Systems. In: F. Kahlen, S. Flumerfelt & A. Alves, eds. *Transdisciplinary Perspectives on Complex Systems.* Basel: Springer International Publishing, pp. 85-113.

Hernández, L. & Hernández, S., 1997. Application of digital 3D models on urban planning. *WIT Transactions on The Built Environment,* Volume 33, p. 395.

Häggblom, K., 2015. *Reglerteknik I Grundkurs.* Turku: Department of Chemical Engineering.

ICCT, 2011. *The Energy Efficiency Design Index (EEDI) for New Ships.* [Online]
Available at: https://theicct.org/sites/default/files/publications/ICCTpolicyupdate15_EEDI_final.pdf
[Accessed 17 December 2019].

IMO, n.da. *Energy Efficiency Measures.* [Online]
Available at:
http://www.imo.org/en/OurWork/Environment/PollutionPrevention/AirPollution/Pages/Technical-

and-Operational-Measures.aspx
[Accessed 17 December 2019].

IMO, n.db. *Sulphur oxides (SOx) and Particulate Matter (PM) – Regulation 14.* [Online]
Available at:
http://www.imo.org/en/OurWork/Environment/PollutionPrevention/AirPollution/Pages/Sulphur-oxides-(SOx)-%E2%80%93-Regulation-14.aspx
[Accessed 18 December 2019].

IPIECA, 2014. *Heat Exchangers.* [Online]
Available at: http://www.ipieca.org/resources/energy-efficiency-solutions/efficient-use-of-heat/heat-exchangers/
[Accessed 26 July 2019].

Manngård, M., 2019. *Personal communication.* Turku: s.n.

Manngård, M., Lund, W. & Björkqvist, J., 2019. On-ship data compression and cleansing using Digital Twins, *Integrated Energy Solutions to Smart And Green Shipping 2019 Edition,* Espoo, 13 March, pp. 41-44. [Online]
Available at: https://www.vttresearch.com/sites/default/files/pdf/technology/2019/T354.pdf
[Accessed 3 March 2020]

Manngård, M., Lund, W. & Björkqvist, J., 2020. Using Digital Twin Technology to Ensure Data Quality in Transport Systems, *Proceedings of 8th Transport Research Arena TRA 2020,* Helsinki, 27-30 April. [Online]
Available at:
https://www.researchgate.net/publication/339875335_Using_Digital_Twin_Technology_to_Ensure_Data_Quality_in_Transport_Systems
[Accessed 18 March 2020]

Mathisen, K. W., Morari, M. & Skogestad, S., 1994. Dynamic models for heat exchangers and heat exchanger networks. *Computers & Chemical Engineering,* 18(Supplement 1), pp. S459-S463.

MathWorks, 2019. *Simulink.* [Online]
Available at: https://se.mathworks.com/products/simulink.html
[Accessed 26 August 2019].

McCabe, W. & Thiele, E., 1925. Graphical design of fractionating columns. *Industrial and Engineering Chemistry,* 17(16), pp. 605-611.

Miskinis, C., 2019. *The history and creation of the digital twin concept.* [Online]
Available at: https://www.challenge.org/insights/digital-twin-history/
[Accessed 24 September 2019].

Monteith, M., 2019. *What Is a Digital Twin?.* [Online]
Available at: https://www.iotforall.com/what-is-digital-twin-technology/
[Accessed 24 September 2019].

Nuclear Power, n.d. *Types of Heat Exchangers – Classification of Heat Exchangers.* [Online]
Available at: https://www.nuclear-power.net/nuclear-engineering/heat-transfer/heat-exchangers/types-of-heat-exchangers/
[Accessed 25 July 2019].

Piascik, B. et al., 2010. *Technology Area 12: Materials, Structures, Mechanical Systems, and Manufacturing Roadmap,* Washington, DC: NASA.

Ramahlingam, T. & Raghavan, V. R., 2011. The Tube Side Heat Transfer Coefficient for Enhanced Double Tube by Wilson Plot Analysis. *Journal of Applied Sciences,* 11(10), pp. 1725-1732.

Scilab, 2019. *Xcos.* [Online]
Available at: https://www.scilab.org/software/xcos
[Accessed 26 August 2019].

Shafto, M. et al., 2010. *Technology Area 11: Modeling, Simulation, Information Technology & Processing Roadmap,* Washington, DC: NASA.

Shah, R. K. & Sekulić, D. P., 2003. *Fundamentals of Heat Exchanger Design.* Hoboken, New Jersey: John Wiley & Sons, Inc.

Shaw, K. & Fruhlinger, J., 2019. *What is a digital twin and why it's important to IoT.* [Online]
Available at: https://www.networkworld.com/article/3280225/what-is-digital-twin-technology-and-why-it-matters.html
[Accessed 24 September 2019].

STI, 2014. *Industrial Heat Exchangers: Design, Construction Types, Service and Maintenance Needs.* [Online]
Available at: https://setxind.com/downstream/industrial-heat-exchangers-construction-types-service-maintenance/
[Accessed 25 July 2019].

U.S. Department of Energy, 1993. *DOE Fundamentals Handbook, Mechanical Science, Volume 1 of 2.* Washington D.C.: U.S. Department of Energy.

Varbanov, P. S., Klemeš, J. J. & Friedler, F., 2011. Cell-based dynamic heat exchanger models—Direct determination of the cell number and size. *Computers & Chemical Engineering,* 35(5), pp. 943-948.

Zou, G. et al., 2013. Modeling ship energy flow with multi-domain simulation, *27th CIMAC World Congress on Combustion Engines*, Shanghai, 13-16 May. [Online]
Available at:
https://www.researchgate.net/publication/257938048_Modeling_ship_energy_flow_with_multi-domain_simulation
[Accessed 17 December 2019]

Figures

Tables

APPENDICES

APPENDIX A

APPENDIX A.1

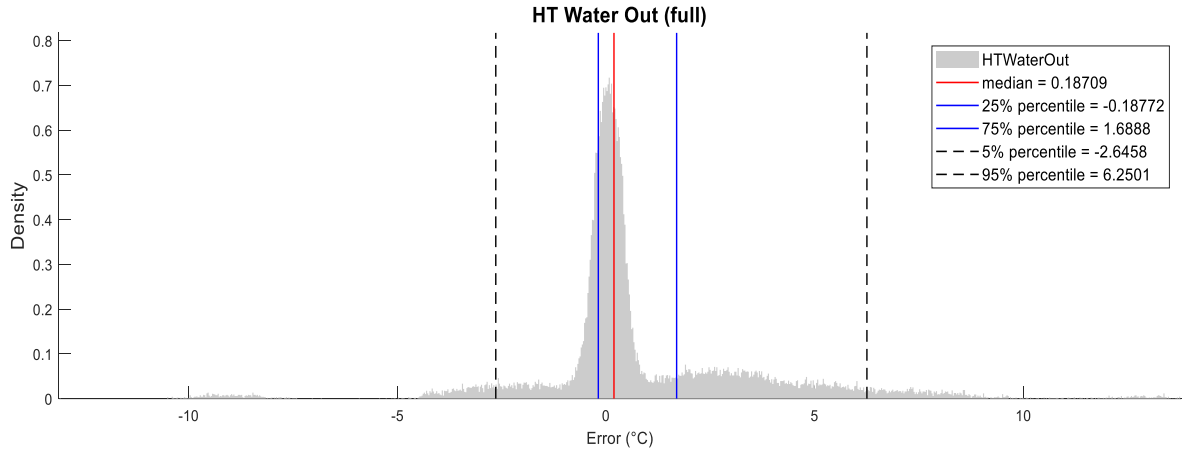

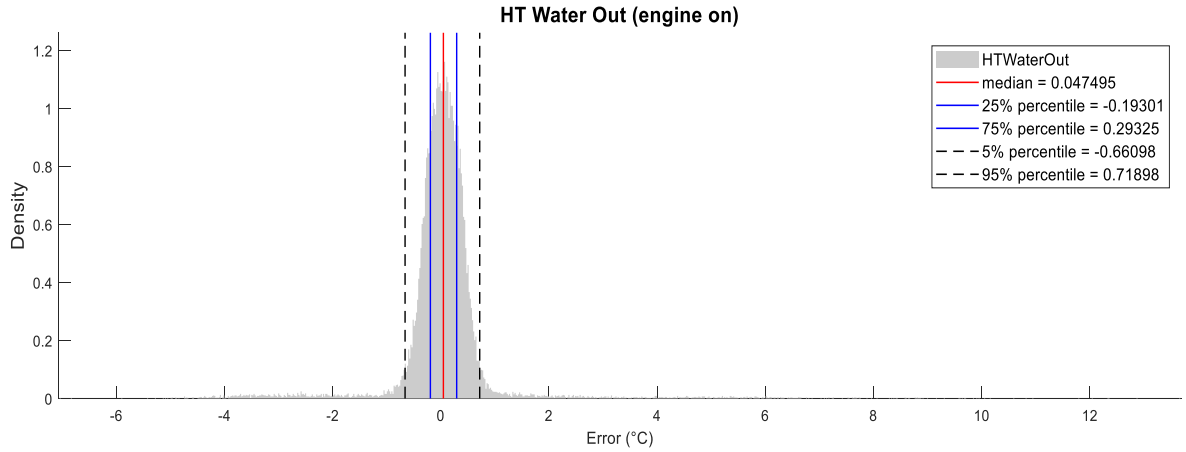

APPENDIX A.2

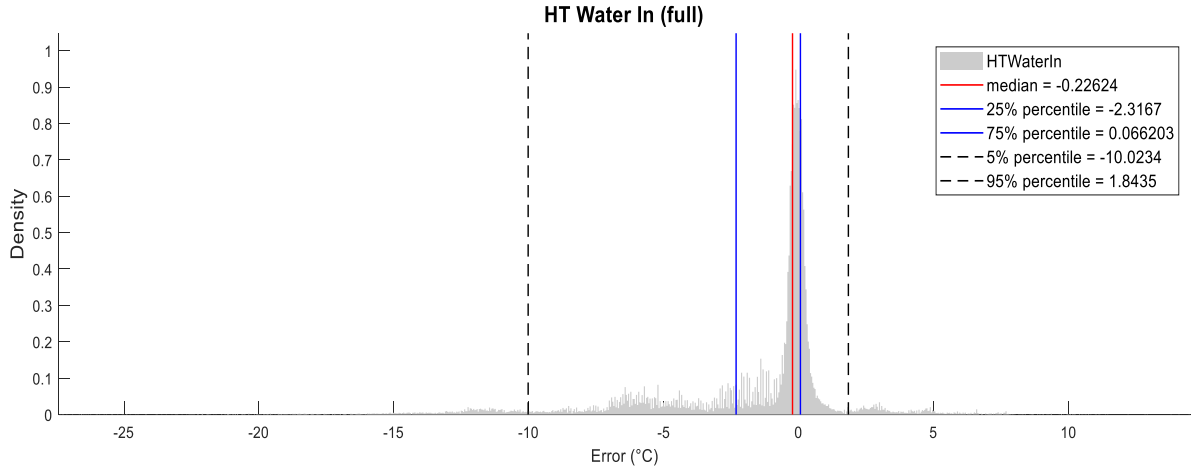
HT Water In (full)
HTWaterIn
median = -0.22624
25% percentile = -2.3167
75% percentile = 0.066203
5% percentile = -10.0234
95% percentile = 1.8435
Density
Error (°C)

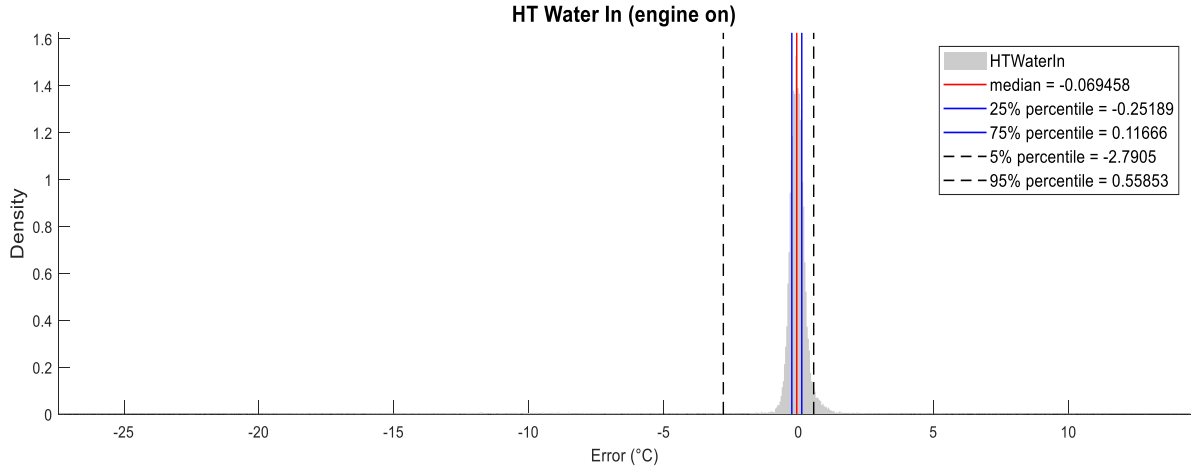
HT Water In (engine on)
HTWaterIn
median = -0.069458
25% percentile = -0.25189
75% percentile = 0.11666
5% percentile = -2.7905
95% percentile = 0.55853
Density
Error (°C)

APPENDIX A.3

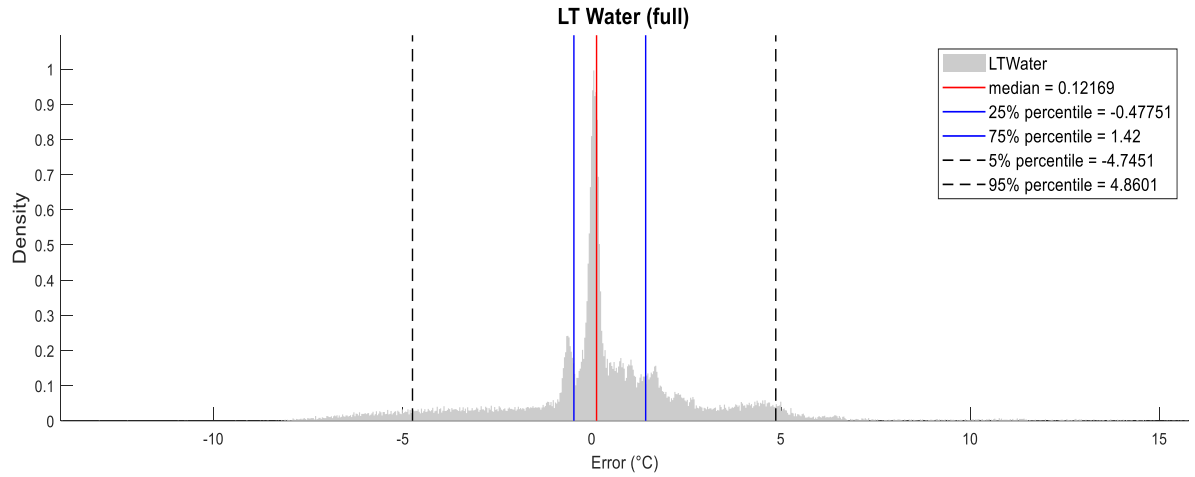
LT Water (full)
LTWater
median = 0.12169
25% percentile = -0.47751
75% percentile = 1.42
5% percentile = -4.7451
95% percentile = 4.8601
Density
Error (°C)

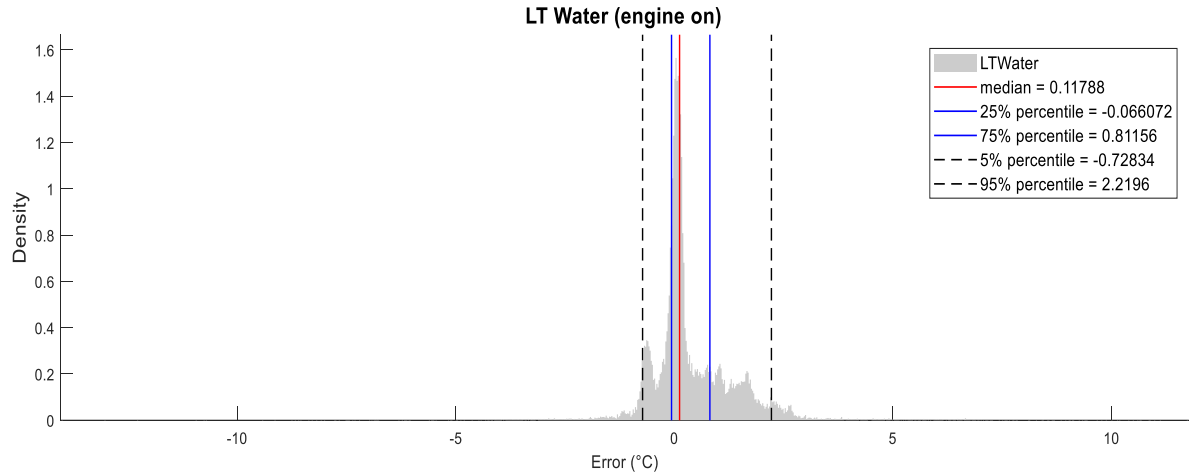
LT Water (engine on)
LTWater
median = 0.11788
25% percentile = -0.066072
75% percentile = 0.81156
5% percentile = -0.72834
95% percentile = 2.2196
Density
Error (°C)

APPENDIX B

APPENDIX B.1

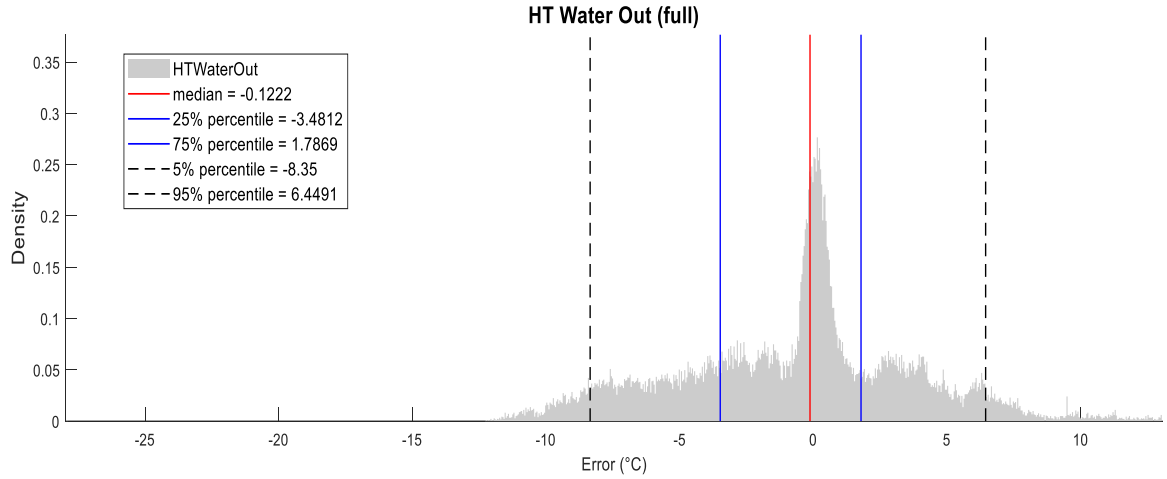

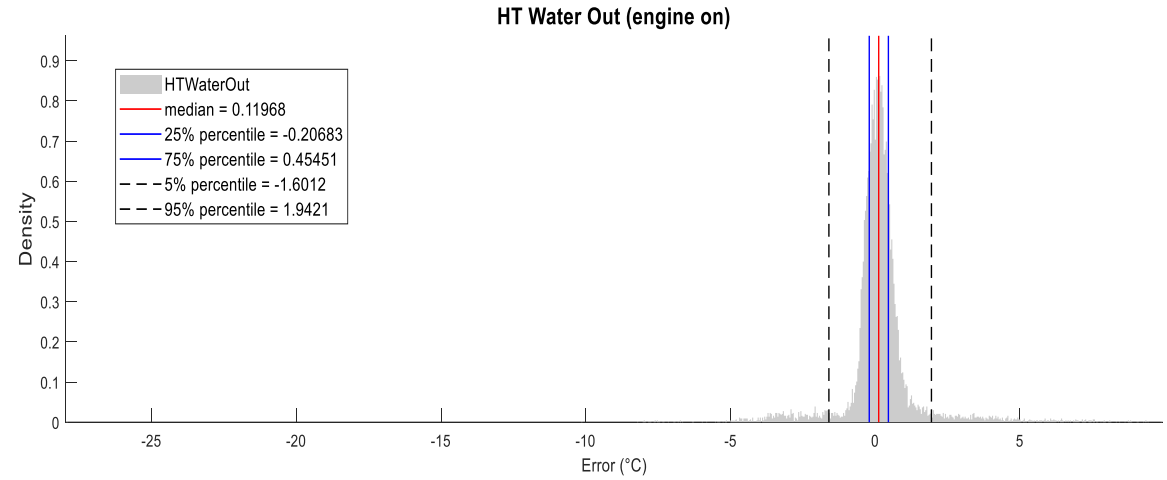

APPENDIX B.2

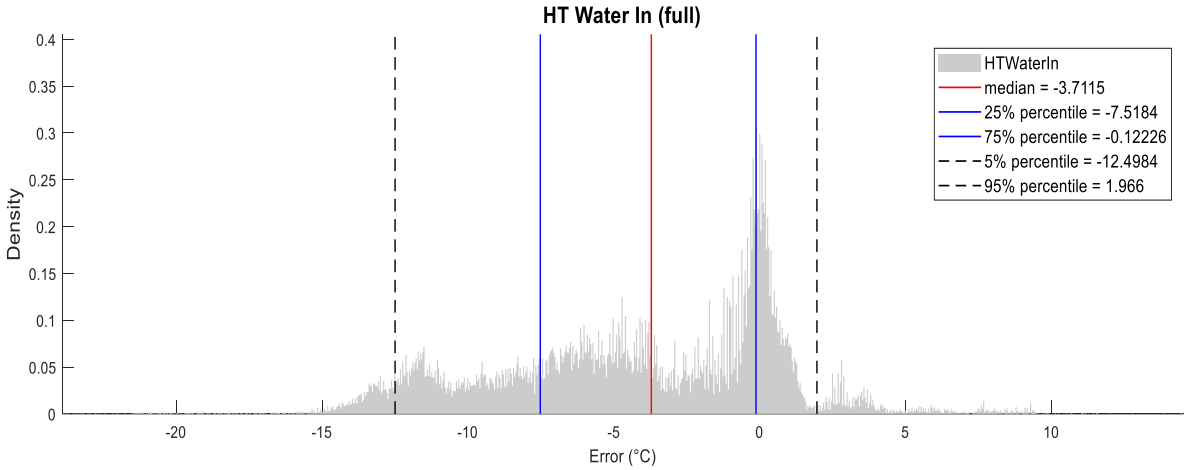
HT Water In (full)
Density
Error (°C)
HTWaterIn
median = -3.7115
25% percentile = -7.5184
75% percentile = -0.12226
5% percentile = -12.4984
95% percentile = 1.966

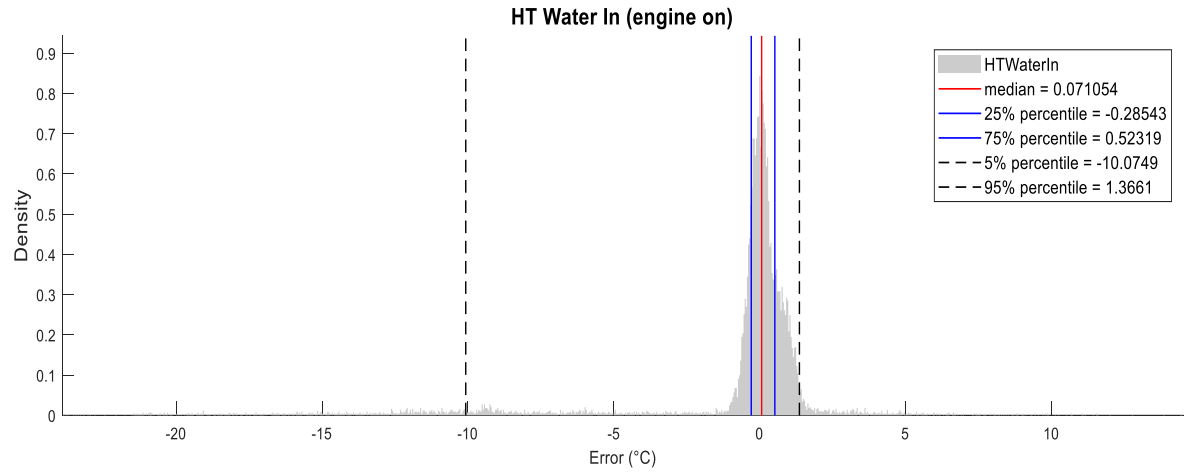
HT Water In (engine on)
Density
Error (°C)
HTWaterIn
median = 0.071054
25% percentile = -0.28543
75% percentile = 0.52319
5% percentile = -10.0749
95% percentile = 1.3661

APPENDIX B.3

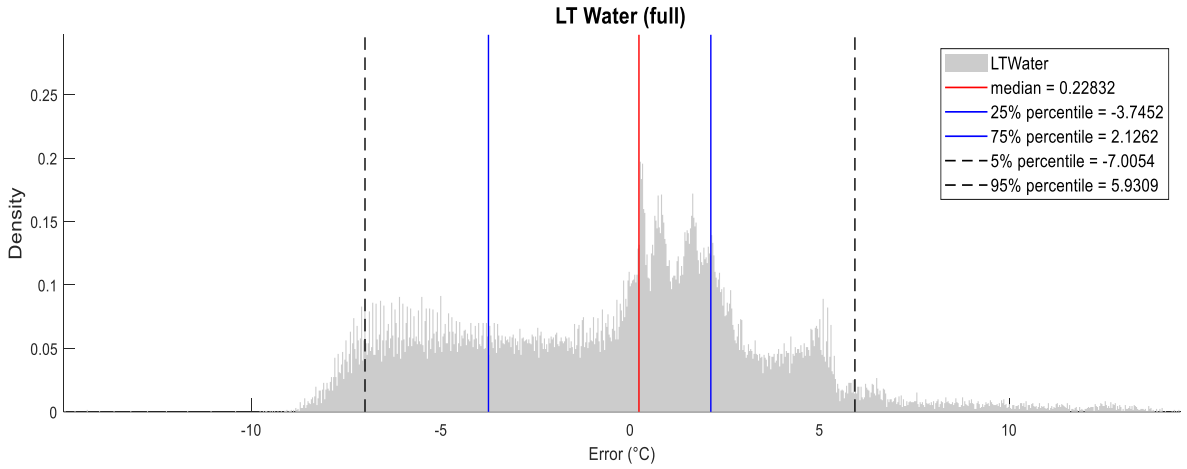
LT Water (full)
LTWater
median = 0.22832
25% percentile = -3.7452
75% percentile = 2.1262
5% percentile = -7.0054
95% percentile = 5.9309
Density
Error (°C)

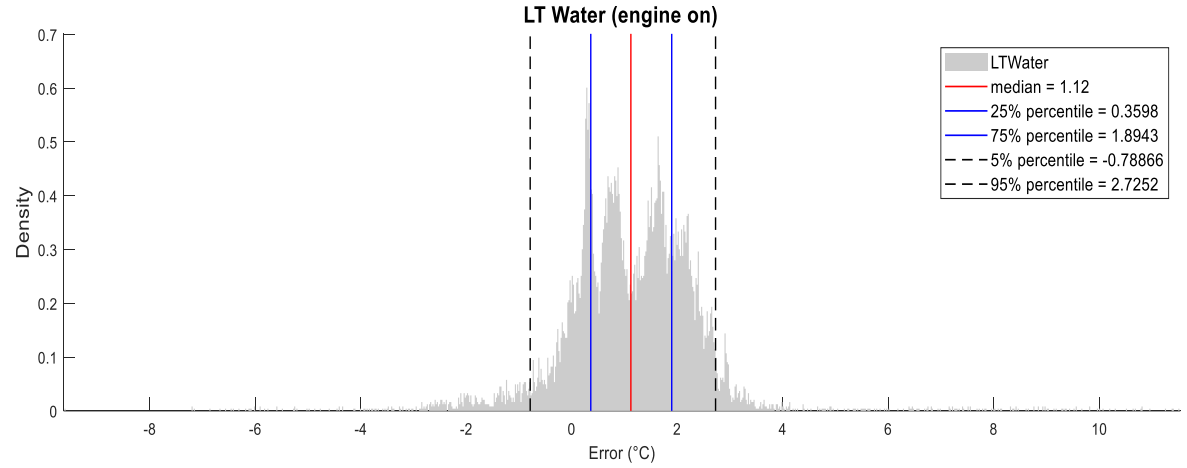
LT Water (engine on)
LTWater
median = 1.12
25% percentile = 0.3598
75% percentile = 1.8943
5% percentile = -0.78866
95% percentile = 2.7252
Density
Error (°C)